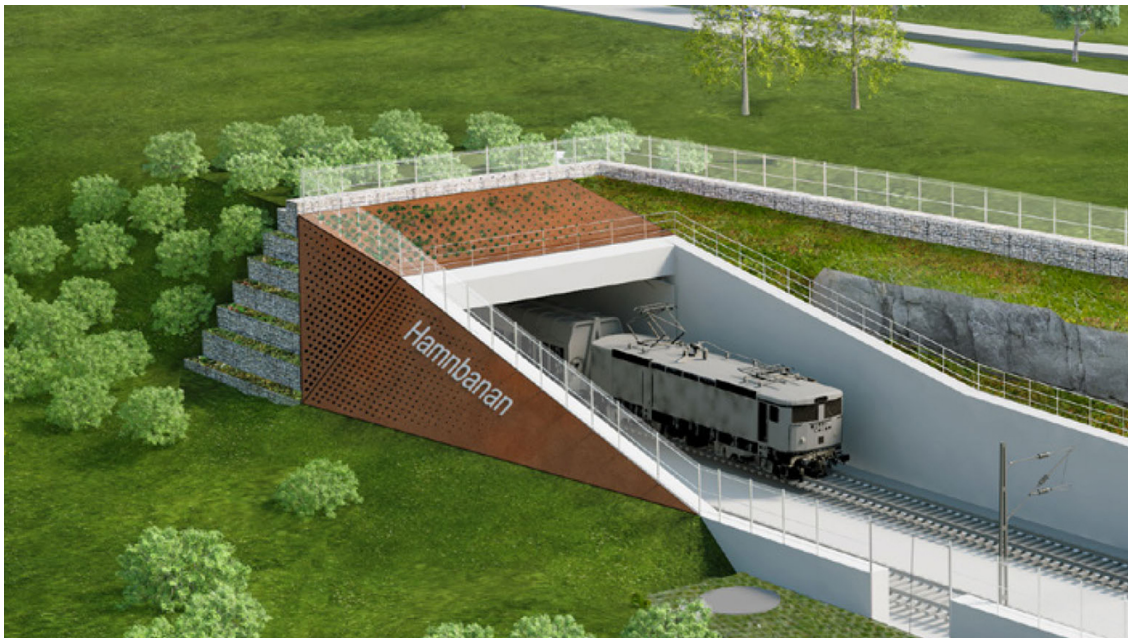


# Assessment of Anchor Forces for a Drilled Pile Wall

An evaluation of the correlation between measured anchor forces, analytical calculations and numerical simulations

Master's thesis in Infrastructure and Environmental engineering

JONAS ERIKSSON
ELIN THULIN

DEPARTMENT OF ARCHITECTURE AND CIVIL ENGINEERING

CHALMERS UNIVERSITY OF TECHNOLOGY
Gothenburg, Sweden 2022
www.chalmers.se

MASTER'S THESIS 2022

# Assessment of Anchor Forces for a Drilled Pile Wall

JONAS ERIKSSON
ELIN THULIN


CHALMERS
UNIVERSITY OF TECHNOLOGY

Department of Architecture and Civil Engineering
*Division of Geology and Geotechnics*
CHALMERS UNIVERSITY OF TECHNOLOGY
Gothenburg, Sweden 2022

Assessment of Anchor Forces for a Drilled Pile Wall
An evaluation of the correlation between measured anchor forces, analytical calculations and numerical simulations
JONAS ERIKSSON
ELIN THULIN



Supervisor: David Ekstrand, Skanska AB
Examiner: Mats Karlsson, Chalmers University of Technology

Master's Thesis 2022
Department of Architecture and Civil Engineering
Division of Geology and Geotechnics
Chalmers University of Technology
SE-412 96 Gothenburg
Telephone +46 31 772 1000

Cover: Illustration of the studied section at Hamnbanan when finished (Trafikverket, 2015).

Typeset in LaTeX
Gothenburg, Sweden 2022

Assessment of Anchor Forces for a Drilled Pile Wall
An evaluation of the correlation between measured anchor forces, analytical calculations and numerical simulations
JONAS ERIKSSON & ELIN THULIN
Department of Architecture and Civil Engineering
Chalmers University of Technology

# Abstract

A large infrastructure project in central Gothenburg, *Hamnbanan*, involves the construction of a new railway that will run throughout the city. The project entails tunnelling through soil as well as rock and aims to increase the capacity of freight train transport headed to and from the port of Gothenburg. The construction of tunnel in soil requires an excavation where an adequate retaining system is essential. A drilled pile wall can be used for friction material where driving a retaining wall in steel can be complicated or not possible. Combined with back-striving anchors as lateral support, a workable excavation process is enabled and is the system used for the reference project in this thesis.

The aim of this thesis was to measure the anchor forces for a specific segment at the project *Hamnbanan* and compare these results to analytical calculations and assumptions. The calculations where carried out in SLS where the wall was modelled with both a free end supported beam and as a free end supported beam with an additional forcing moment. Furthermore, it was analysed how a drilled pile wall can be modelled in a 2D numerical program to account for the embedded support in rock. This was accomplished by correlating numerical anchor forces with site-measured values. By pre-stressing the two walls to different lock-off loads, the anchor loads could be evaluated over time.

The results shows that a reduced lock-off load causes a larger variation in anchor force during excavation although no anchor reached the originally designed lock-off load. It can be seen how blasting inside the excavation increases all measured values except the ones that are lowered to a greater extent. When a free end support is assumed the analytically calculated results are significantly higher than the measured results. For a free end support with a forced moment at the support, the analytic results correlate to a greater extent and it is considered more adequate. An evaluation is made on how to model a drilled wall into rock in a numerical geotechnical program by resemble the numerical anchor forces to measured values. It is stated that a lower strength material around the embedded section of the wall foot is the method with the most coincident results.

To conclude the thesis, load-bearing structures can be optimised by utilising the moment capacity of a drilled pile wall when designing a retaining system. When modelling a geotechnical problem, a numerical model can be useful, and the embedded section in the rock for a drilled pile wall must be carefully examined.

**Keywords:** *Anchors, Retaining walls, Load loss, Drilled pile wall, Sheet pile wall, Anchor methods, Finite element method, PLAXIS 2D, Hardening Soil Model.*

# Acknowledgements

First of all, we would like to sincerely thank our supervisor David Ekstrand at Skanska for excellent guidance, good ideas and patience throughout the whole process. Secondly, we would like to thank Mats Karlsson at Chalmers University for good conversations and insights in the topic. We would also like to give our appreciation to Valeria Håkansson and her team at the Hamnbanan project for making us feel welcome and assisting us with installation of equipment and measurements on site.

Finally, we'd like to express our gratitude to our fellow students at Chalmers for making these five years memorable and enjoyable. A special thanks to our friends for support and entertainment throughout the whole pandemic, as well as this thesis.

Jonas Eriksson & Elin Thulin, Gothenburg, 2022

# Acronyms & Variables

Below is the list of acronyms that have been used throughout this thesis listed in alphabetical order:

## Acronyms

| | |
|---|---|
| ALC | Anchor Load Cell |
| Hfa | Ram sounding test |
| CPT | Cone Penetration Test |
| ANP anchor | Anchor Nail Pile - Anchor |
| ULS | Ultimate Limit State |
| SLS | Serviceability Limit State |
| ALS | Accident Limit State |
| MC | Mohr Coulomb |
| HS | Hardening Soil Model |

## Variables

The Following are the variables of indices, sets and parameters that have been used throughout this thesis.

### Hydrogoelogy

| | |
|---|---|
| GW T50$_{min}$ | The minimum groundwater level after a 50-year rain |
| GW T50$_{max}$ | The maximum groundwater level after a 50-year rain |

| | |
|---|---|
| $GW_{medel}$ | The average value of the groundwater level after a 50 -year rain |

## Partial coefficients

| | |
|---|---|
| $\gamma_M$ | Material |
| $\gamma_d$ | Model factor |
| $\gamma_{s,da}$ | Model factor for active pressure |
| $\eta$ | conversation factor |

## Soil parameters

| | |
|---|---|
| $E$ | Young's modulus |
| $E_0$ | Initial Young's modulus |
| $E_{50}$ | Young's secant modulus for 50% of the maximum devatoric stress |
| $E_{ur}$ | Young's modulus for unloading- reloading |
| $E_{oed}$ | Young's modulus for primary oedometer compression test |
| $G$ | Shear modulus |
| $\nu$ | Poisson's ratio |
| c | Cohesion |
| $\phi$ | Friction angle |
| $\psi$ | Dilatancy angle |
| $\gamma_{unsat}$ | Unsaturated unit weight |
| $\gamma_{sat}$ | Saturated unit weight |
| $c'$ | Effective Cohesion |
| $\tau_f$ | Shear strength due to friction? |
| $\sigma$ | Total earth pressure |
| $\sigma'$ | Total effective earth pressure |
| $\sigma_0$ | Initial earth pressure |
| $\sigma_h$ | Horizontal earth pressure |
| $\sigma_v$ | Vertical earth pressure |
| $u$ | Pore pressure |
| $K_0$ | earth pressure coefficient |
| $f_{yk}$ | Yield strength capacity |

| | |
|---|---|
| $f_{uk}$ | Tension strength capacity |
| $K_A$ | Active earth pressure coefficient |
| $K_P$ | Passive earth pressure coefficient |
| $P_{netto}$ | Net earth pressure |
| $P_A$ | Active earth pressure |
| $P_k$ | Passive earth pressure |
| $P_{a,net}$ | Active net earth pressure |
| $P_{p,net}$ | Passive net earth pressure |
| $M_q$ | Moment around waler beam |
| $M_{fixed}$ | Moment at the foot of the partially fixed support |
| $M_{free}$ | Moment at the foot of the wall for a free supported wall |
| $M_{Rd}$ | Bending moment capacity |
| $M_{Ed}$ | Design bending moment of the wall |
| $T_{Ed}$ | Design shear force |
| $T_{Rd}$ | Shear force capacity |
| $q_{dovel}$ | The load uptaken by a wall dovel |
| $q_h$ | Waler beam force in horizontal direction |
| $q_{h,45}$ | Waler beam force in a 45 $^\circ$ inclination |

# Contents

# List of Figures

# List of Tables

# 1
# Introduction

Large infrastructure projects in densely populated areas have limited construction space while still requiring deep excavations. Ground movement and fluctuations in groundwater level must be kept to a minimum due to the close proximity to houses and other structures. By using retaining walls, a safe excavation is enabled with less space consumed, compared to using slopes to reach the desired level. The retaining walls can be supported by both horizontal struts or by back-striving anchors which are usually made of steel (Keller Group, 2022). In Sweden, anchors are a common method which enables an open excavation and easy access for following work to be executed. The retaining wall can be made of a variety of materials, including concrete, wood, or steel, with steel being the most commonly used one (Keller Group, 2022).

Gothenburg, Sweden's second largest city, is undergoing a major infrastructure project to lower the existing railway connection from the port through densely populated areas of the city, known as the Hamnbanan route. This entails a cut-and-cover concrete tunnel, as well as, a tunnel through rock. The project requires a sufficient retaining system because it involves long distances of excavation through populated areas with an existing railway nearby. It is critical to ensure that the retaining system's strength is adequate, and anchor forces can play a role in this. The method of calculation can be confirmed by comparing measured anchor forces to the design value.

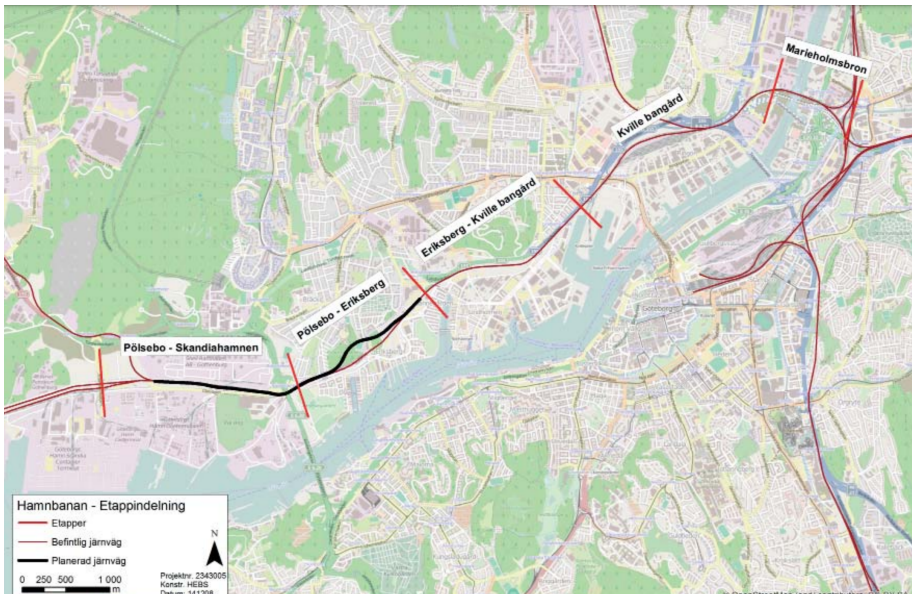


**Figure 1.1:** Overview over Gothenburg and the location of *Hamnbanan*

A great amount of the emissions from a large infrastructure project such as *Hamnbanan* comes from material transportation from and to the site, as well as the significant amount

of material used for retaining systems and the tunnel itself. Therefore, the emissions could be decreased if the amount of material could be reduced. In the construction industry, steel and concrete are used as building materials and for both permanent and temporary constructions. Steel retaining structures account for a significant portion of the total amount of steel used in infrastructure projects. Steel has an impact on emissions in Sweden in general, with the steel industry accounting for 31% of the country's annual CO2 emissions (Naturvårdsverket, 2022).

## 1.1 Aim and Objectives

The aim of this thesis is to assess measured anchor forces with analytical calculations and results from finite element method. By doing this the analytical calculation method can be validated and correlated to anchor forces for a drilled pile wall. The assessment is also done by investigating how the retaining system can be modeled in a finite element program that corresponds to the measured values. Furthermore, it is evaluated if the anchored system can benefit from a drilled pile wall in terms of an anchor force and thereby to optimize the amount of steel used.

The aim of this report consolidate to the following research questions:

- What are the measured anchor forces on site for drilled pile walls and how does these correlate to analytical results?
- How can a drilled pile wall be modelled in a numerical program that corresponds to the measured values?
- How does the lock off load affect the anchor forces during excavation?
- Can a drilled pile wall be beneficial in terms of reducing steel amount with respect to anchors forces?

## 1.2 Limitations

The following limitations where done to perform this thesis:

- Only retaining systems in steel will be considered. For example, this means that diaphragm walls or secant piles will not be considered.
- The components of the retaining systems and their dimensions are retrieved from the design of the project and are not considered to be changed.
- Only back-striving anchors fixed in rock are modelled and calculated for.
- Calculations are performed for two dimensions and only horizontal isotropic layers for soil and rock are considered.
- External influence on the performed measurements in field are not considered, such as temperature and precipitation.

## 1.3 Method

This thesis is initiated with a litterateur review of scientific papers and of previous work regarding the subject. This is in order to get an understanding of the theory behind temporary constructions and specifically back-striving anchors. Furthermore, the literature provided knowledge about the different material models used in PLAXIS and how to model the studied case in the most suitable way. The main search portals for articles is *Google scholar*, *Science Direct* and *Chalmers library portal*.

For analytical calculations *Microsoft Excel* version 2203 is used. For Numerical modeling and finite element calculations of the excavation, the geotechnical analysis software *PLAXIS 2D*, version 21.00.01.7, is used. To calculate anchor forces, the sectional forces are extracted through a 2D structural design software, *Frame Analysis 6.5*, issued by *Strusoft*. The program uses 1 and 2nd order theory to solve problems for plane structures (StruSoft, 2022).

The data is collected using anchor load cells and the readings are carried out during the spring of 2022. Values for a whole excavation process can be analyzed. Data of soil and material properties are collected by Skanska who is the main contractor of the project Hamnbanan and has done the design of the temporary constructions as well as the tunnel. The geotechnical data is performed by another company and is evaluated by Skanska.

The initiated literature review is followed by a description of the case study and the investigated project specific section. Then the model in PLAXIS and the analytical calculations are presented and described which then leads to the chapter presenting the results. The thesis is then lastly completed with a discussion of the results and proposals of further research. The method for this study can be divided into three sections, each presented in the following chapters. The conceptual model used for the study is visualized in Figure 1.2.

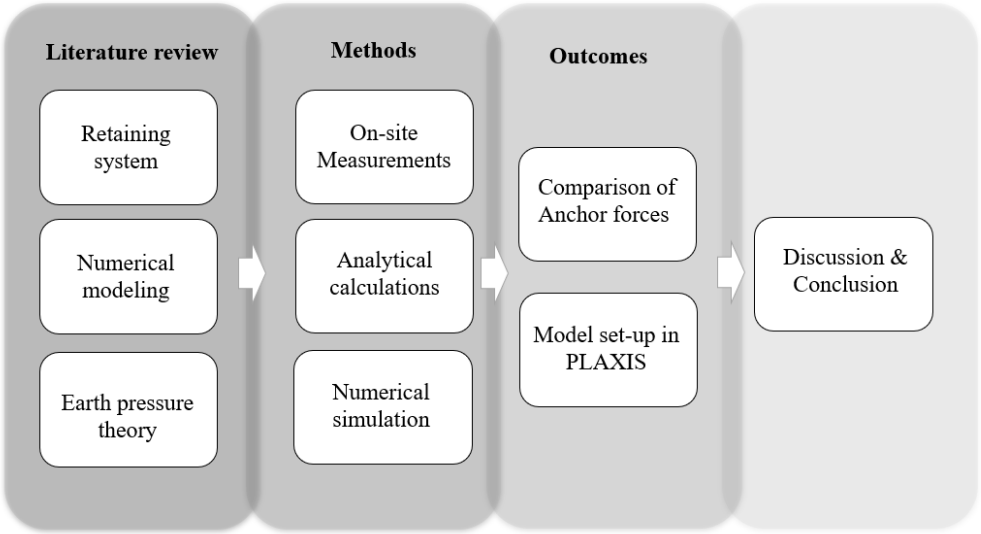


**Figure 1.2:** Conceptual model of the method presented for the study.

# 2
# Literature Review

For this section the underlying theory for earth pressures are presented as well as some important soil properties. Furthermore, the main components for a retaining system of steel presented and similar studies are reviewed.

## 2.1 Earth Pressure Theory

There are several methods and theories for calculating earth pressures and the lateral pressure acting on a retaining wall and they will not all be covered in this thesis. The understanding of the underlying theory is important for both the analytical calculations and for the input data in the finite element analysis.

The analytical calculation in this thesis is based on *Sponthandboken* (Fredriksson, Kullingsjö, Ryner, & Stille, 2018) and the Swedish standards. Those in turn, are based on Rankine´s earth pressure theory and Mohr Coulomb's failure criteria which is covered further in the following sections.

The effective stress in soil can be described as the force obtained by the skeleton of the soil fractions. In 1943 Terzaghi presented his relationship between the total stress, pore pressure and total effective stress:

$$\sigma = \sigma' + u \tag{2.1}$$

Friction materials such as sand and gravel have small connections which implies that they have a large void ratio. This causes the material to have less inbound water compared to cohesion material and to be more permeable. This entails that the pore pressure is of great importance for the effective stress where the stress is lower below the groundwater level. Furthermore, when analysing friction material the cohesion is assumed to be zero below the groundwater level, therefore called cohesion-less material (SGI, 2022). Although, when analysing cohesion-less material by using finite element method programs a small cohesion value is recommended to apply close to the surface in order for the program to function properly (Bentley Systems, 2021).

### 2.1.1 Mohr Coulomb's Failure Criteria

Assuming simply elastic behaviour would imply that the soil is infinitely strong, which is not the case. If the shear stresses reaches the materials shear strength, shear failure will occur. Originally Coulomb proposed that the limiting strength of soils was purely frictional and where T is the limiting frictional force (Knappett & Craig, 2012). The friction is then often described as the acting normal force multiplied with a friction factor.

To apply this equation to soil, it is more appropriate to write the Equation as 2.2 shows where tan($\phi$) is equivalent to the friction coefficient (Knappett & Craig, 2012).

$$T = \mu \cdot N \Rightarrow \tau = \tan\phi \cdot \sigma \tag{2.2}$$

Assuming two dimensional stress state the Mohr Coulomb model presents a plot with shear stress, $\tau$, against effective normal stress $\sigma$'. A stress state for a particle can be described either through pairs of coordinates or through the Mohr Coulombs failure envelope, see figure 2.1, that is descried through the principal effective stresses, $\sigma'_1$ and $\sigma'_3$.

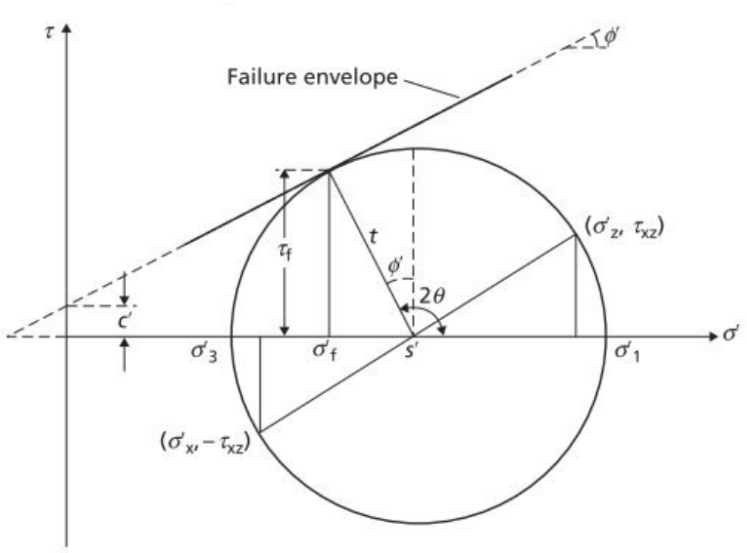


**Figure 2.1:** Mohr Coulombs failure envelope (Knappett & Craig, 2012).

The circle represents all possible stress states on all possible planes for the particle and failure will occur when the circle touches the failure envelope (Knappett & Craig, 2012). The failure envelope is based on the friction model seen in equation 2.2. To account for the interlocking between grains the envelope is approximated to a linear graph and evaluated as equation 2.3.

$$\tau_f = c' + \sigma' \cdot \tan(\phi') \tag{2.3}$$

It should be approximated that c´and $\phi'$ are mathematical constants creating a linear assumption and failure will occur where a critical combination of these develop. It should be noted that the cohesion, c', and friction angle, $\phi'$, is given in effective terms. This is done by eliminating the additional strength from the water in the material, assuming that the material is drained. If the material is undrained the water need to be considered, this can be done by using the total strength. The Mohr Coulomb failure criteria can still be used but modified with $c_u$ and $\phi_u$ (Knappett & Craig, 2012).

### 2.1.2 Rankine's Theory

Rankine proposed that the earth pressure limits was in a state of plastic equilibrium. His theory attend three conditions: the earth at rest, the active pressure and the passive. The acting load depends on the movement of the wall and the initial earth pressure, $\sigma_0$. Through general strength parameters, $\phi'$ and c', Rankine developed a lower bound solution where shear failure will occur along a plane at an angle of $45°$ + $\frac{\phi'}{2}$ where Mohr´s circle represent the state of stress failure. The theory states that two points can only develop equilibrium when some deformation in the soil mass takes place (Knappett & Craig, 2012).

### 2.1.3 Young's Modulus, E

Prior to the plastic failure the soil behave like an elastic constitutive model. The modulus can often be described through the ratio between deviatoric stress and strain. To simplify, the soil can be approached as linear elastic where the shear strain is directly related to the applied shear stress. But the stress may also be effected by normal stress components and for a linear constitutive model the relationship can be given by Hooke's law. When the soil remains elastic the determination of the soil response to stress requires elastic properties such as Young's modulus, E and Poisson's ratio (Knappett & Craig, 2012).

As the stiffness of soil depend on the stress level the Young's modulus needs to be evaluated based on the studied case (Bentley Systems, 2021). As many materials shows a non-linear relationship there are several modifications for the stiffness modulus for different material models. For materials with a high elastic behavior in the beginning of a loading test it is reasonable to use $E_0$ as initial modulus or the secant modulus, $E_{50}$, describing as 50% of the load capacity. Tunnels and excavations are an unloading problem hence the modulus for unloading-reloading, $E_{ur}$, can be of interest .

### 2.1.4 Dilatancy & Friction Angle

The main parameter for evaluating friction materials strength capacity is the friction angle which in turn depends on the void ratio, material composition and och anisotropy (Larsson, 1989). As stated from the Swedish Geotechnical Institute, SGI, the friction angle is correlated with the stress in the soil where the strength decreases with an increased normal stress (Larsson, 1989).

The dilatancy is describing the change in volume for a granular material due to rearranged grains when the soil starts to shear. The dilatancy in sand depends on the density and the friction angle. For very loose sands the dilatancy angle can be assumed to be zero, and the same applies for cohesion materials. When the dilatancy angle is positive it implies that, in drained conditions, the material will continue to dilate as long as shear deformation occurs in the material (Bentley Systems, 2021). For undrained calculations the dilatancy angle can cause an over-prediction in the strength of the soil. Solid soils with low tension have the highest dilatancy (Larsson, 2008). The angle of dilation ($\psi$) is defined as: $tan^{-1}(d\varepsilon_v/dy)$ and can be determined through shear tests of loose and dense packed sand tests where the final angle depends on the void ratio thus this describes how much space

the grains can dilate on. The angle of dilation is determined through the average of all particles for the specimen.

The ultimate values of material strength parameters are equal for loose and dense sands but the peak can vary depending on the initial particle density. In dense soils the maximum angle of shearing, $\phi'_{max}$, resistance capacity is much greater than for loose sands (Larsson, 1989).

## 2.2 Acting Earth Pressure

The pressure acting on a retaining wall is the horizontal contribution from the soil and external load such as traffic loads and surrounding buildings.

The pressure acting horizontally on the wall towards the excavation pit can be described as active earth pressure. It is the pressure driving the retaining wall towards failure, see Figure 2.2. The active earth pressure can be explained through the horizontal stress as: $p_a$ = $\sigma_h$ where $\sigma_h$ can be evaluated as:

$$\sigma_h = \sigma_v \cdot K_0 \tag{2.4}$$

Where $K_0$ is the earth coefficient at rest and can for friction material be evaluated through Jaky's Equation: $K_0 = 1 - sin(\phi)$

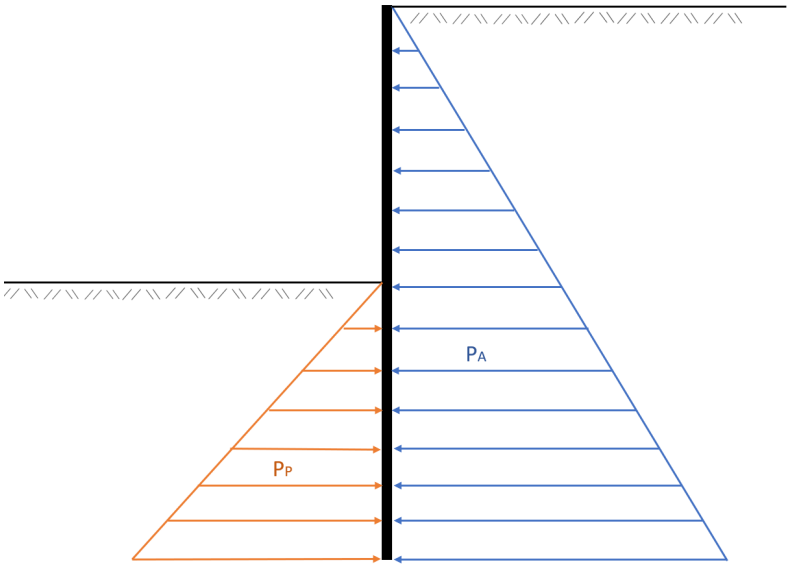


**Figure 2.2:** Active and passive pressure acting on the retaining wall.

The pressure that acts resisting against failure, often on the inside of the excavation is called the passive earth pressure, see Figure 2.2. Some movement in the retaining wall is necessary for passive earth pressure to be able to establish, though this is not required for the active pressure (Fredriksson et al., 2018). Small deformations utilize less of the soils strength which means that the retaining wall need to handle larger pressures. On the other

hand, if the deformations are large and the soil is fully, or almost fully utilized the lateral pressure acting on the retaining wall is calculated using Mohr Coulombs equations for the pressure coefficient, $K_a$ and $K_p$ (see Equation 2.5 and 2.6) which can be used for friction material with an horizontal surface. For an inclined surface, see Section 2.2.1.

$$K_a = \frac{1 - \sin(\phi)}{1 + \sin(\phi)} = \tan^2(45 - \frac{\phi}{2}) \tag{2.5}$$

$$K_p = \frac{1 + \sin(\phi)}{1 - \sin(\phi)} = \tan^2(45 + \frac{\phi}{2}) \tag{2.6}$$

The pressure coefficients are then multiplied with the vertical stress. Based on Terzaghi's principle, the active and passive pressure can therefore be calculated through Equation 2.7 and 2.8, respectively. Furthermore, assuming that the retaining wall is closed against intrusion there will be an pressure acting on the retaining wall originated from the water in the soil. As the same principle as active and passive pressure the water below excavation surface will start to work favourably for the retaining wall.

$$P_a = K_a \cdot \sigma'_v(z) + u(z) \tag{2.7}$$

$$P_p = K_p \cdot \sigma'_v(z) + u(z) \tag{2.8}$$

The earth pressure that is acting on the retaining wall can be hard to estimate. It depends on the the walls stiffness and the integration between the soil and the wall. The stiffness of the retaining wall affect the force in the support and the walls moment. The complexity of the interaction results in empirical factors used to adjust the pressures of the soil in order to simplify the analytical calculations (Fredriksson et al., 2018).

Rankine's theory does not cover the interaction between the wall friction and the soil which Mohr Coulombs theory does. Although later modifications done to Rankine´s equation does. In most real cases the wall will not be completely smooth and some shear stress will be generated for the soil-wall interface. This implies that along the surface the stresses will be acting in the opposite direction to the principle total stresses. For analytical calculation is it common to assume a smooth wall, and if not a common value can be used thus it is complex to know the exact roughness of the wall.

### 2.2.1 Inclined Ground Surface

Rankin's theory assumes that the ground is flat on the retained side. However, in real life it is common that there is a slope ending at the wall. Mohr Coulomb's equations for the active and passive coefficients considers this according to Equation 2.9 and 2.10, respectively.

$$K_a = \frac{\cos^2(\phi' - \omega)}{\cos^2\omega \cdot \cos(\phi'_a + \omega) \cdot \left(1 + \sqrt{\frac{\sin(\phi'+\phi_a)\cdot\sin(\phi'-\alpha)}{\cos(\phi'_a+\omega)\cdot\cos(\alpha-\omega)}}\right)^2} \tag{2.9}$$

$$K_p = \frac{\cos^2(\phi' + \omega)}{\cos^2\omega \cdot \cos(\omega - \phi'_a) \cdot \left(1 - \sqrt{\frac{\sin(\phi'+\phi_a)\cdot\sin(\phi'+\alpha)}{\cos(\omega-\phi'_a)\cdot\cos(\alpha-\omega)}}\right)^2} \tag{2.10}$$

where:
$\phi'$ is the materials frictions angle
$\lambda$ is the inclination of the retaining wall towards the shaft
$\phi'_a$ is the soil's friction against the wall
$\alpha$ is the inclination of the slope of the surrounding soil surface against the retaining wall

The inclined ground surface contributes with a shear force acting on the retaining wall due to it´s slip surface. Elasticity theory by Bouissinesq or Fröhlich e.g can also be used for a permanent or temporary load, where the soil of the slope can be seen as a permanent load. The elasticity theory assumes an ideal elastic and homogeneous soil where a factor, n, takes the increased modulus of strength into account (Bergdahl, Ottosson, & Stigson Malmborg, 1993). Although, the elasticity theory for the calculations are considered not enough sufficient to be used for this case study.

Instead the slope of the surrounding surface can be accounted for by modifying the active earth pressure coefficient, $K_a$, by the relationship between the friction angle and the inclination of the slope, $\beta$, as can be seen in Figure 2.3 below (Swedish Standard Institute, 2022). The slopes are based on Mohr Coulomb theory and Equation 2.9 and 2.10.

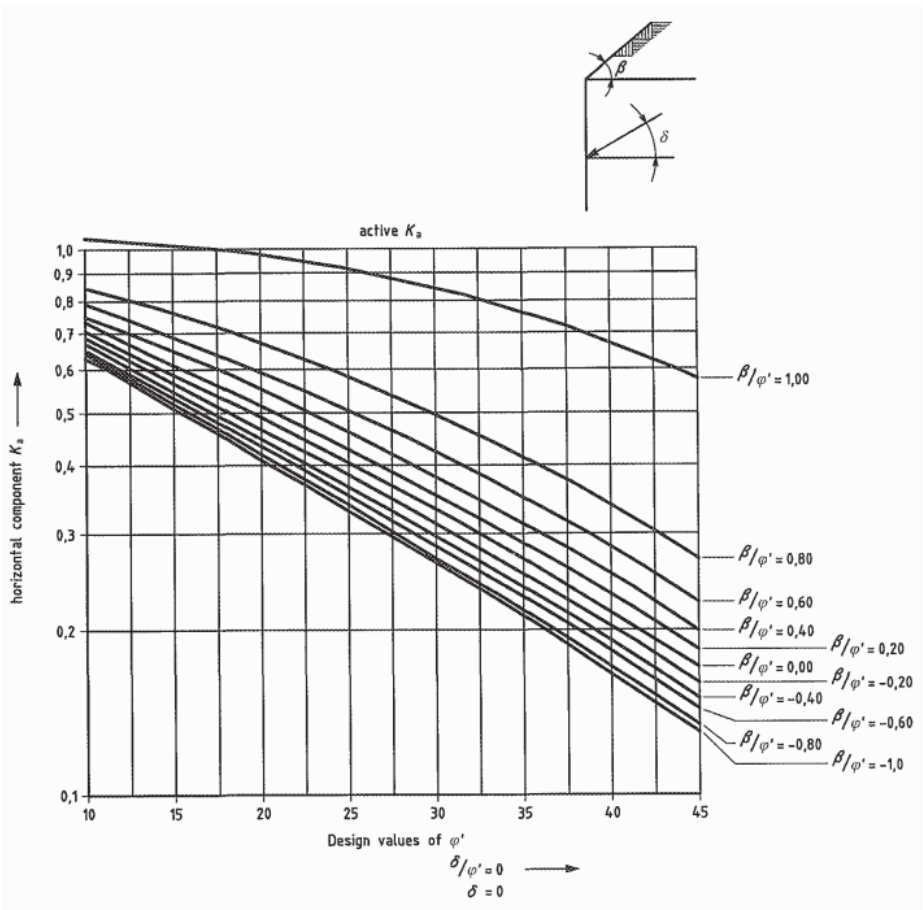


**Figure C.1.2 — Coefficients $K_a$ of active earth pressure: with inclined retained surface ($\delta/\varphi' = 0$ and $\delta = 0$)**

**Figure 2.3:** Used graph's for evaluating the $K_a$-value based on the friction angle and inclination of slope (Swedish Standard Institute, 2022).

## 2.3 Steel Retaining Walls

Retaining walls are commonly used to laterally support the surrounding soil of constructions to enable excavations or to change the level of the ground. The alternative would require a slope with an sufficient inclination which would be space consuming. In addition to the strength of the wall it is important that they minimize the ground movement and prevent intrusion or lowering of groundwater levels. There are several methods and materials for constructing a retaining wall and they all have different characteristics and areas of application. Retaining walls can generally be used as both temporary and permanent constructions, where permanent walls are often a part of the final design (Knappett & Craig, 2012). Retaining walls made out of steel are commonly used as a temporary retaining wall for construction projects due to their effective installation and the flexibility in shape and length.

### 2.3.1 Sheet Pile Walls

Sheet piles are either drived or vibrated into the ground. By connected joints with the adjacent walls the construction provides structural resistance and a relatively waterproof construction. Sheet piles are advantageous since they can be re-used when the final construction is finished and the length can easily be adjusted. On the other hand, the driving or vibration of the sheet pile can be obstructed by boulders or gravels in the soil. The wall can be floating in the soil or drived to rock surface. To counteract the risk of gliding against the bedrock the sheet piles can be supplemented with rock dowels which can assimilate lateral force. The dowel is installed next to the wall before excavating is initiated.

There are several different profiles of sheet piles where the U-profile and Z-profile are two commonly used, see Figure 2.4.

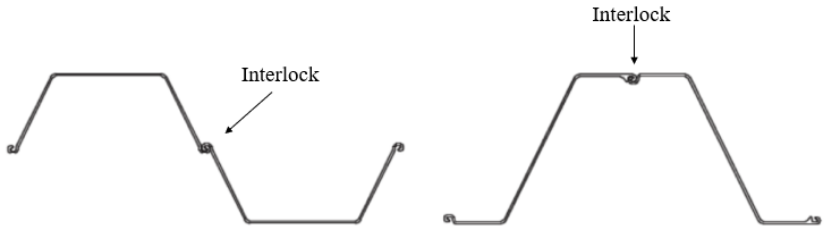


**Figure 2.4:** U-profile (left) and Z-profile (right) of sheet pile wall.

Both profiles are used for deep excavations and tied back walls. The U-profile interlocks with adjacent piles at the neutral axis of the wall which creates a risk of sliding at the connection and therefore the profile has a lower bending moment, compared to the Z-profile. Although, due to its narrow section it creates a wall with high drivability and re-usability. The Z-wall is locked symmetrically and therefore it has a higher bending moment and ensures an effective shear transmission (GIKEN LTD, 2022). On the other hand, the U-profile has a larger tolerance against differences in water pressure acting on the sheet pile (Fredriksson et al., 2018).

### 2.3.2 Drilled Pile Wall

If the soil is sensitive or if it contains larger blocks it can be hard to drive or vibrate sheet piles. In such case drilled steel piles can be used instead. The piles can either be drilled to create a continuous wall or to create a sparse one. A continuous wall is, just like the sheet pile wall, connected with the adjacent piles through welded interlocking sections, see Figure 2.5 and creates a retaining structure, stable against both horizontal and vertical loads (SSAB AB, 2022). For a sparse wall, or "Soldier pile wall", the piles are installed with an open distance to each other. If needed, the soil in between can be supported through metal plates, concrete or other soil strengthening methods before or during the excavation process, see Figure 2.6.

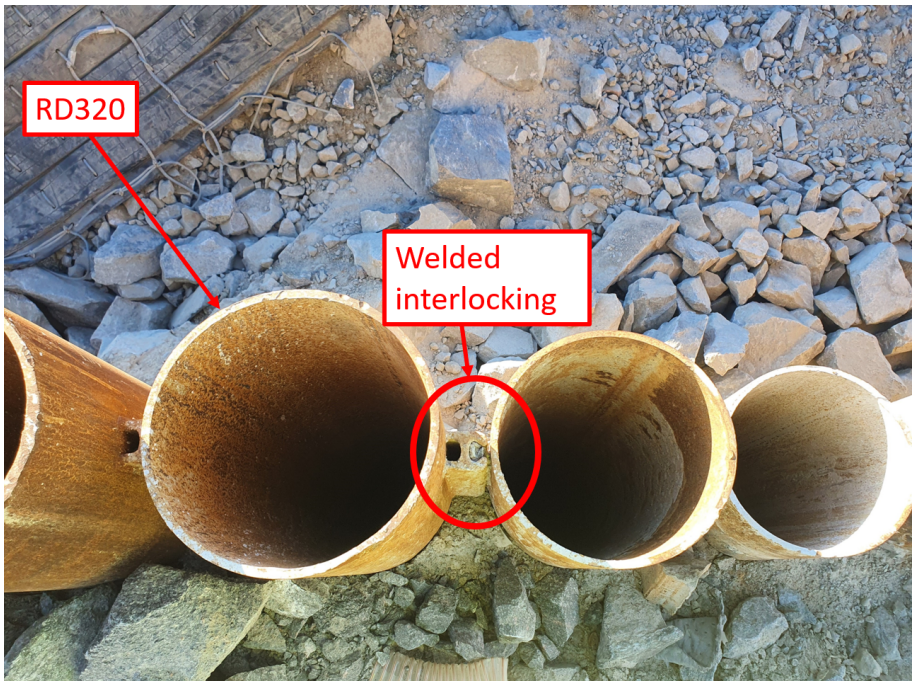


**Figure 2.5:** Drilled pile wall with intersections, RD-wall.

**Figure 2.6:** Sparse wall or "soldier pile wall", from the studied site.

Because this type of retaining wall is drilled into rock the risk of sliding is rapidly lowered and no preventing measurements are necessary. Instead the wall can be seen as having a fixed-end, or partially fixed. This needs to be considered in calculation as it lowers the maximum field moment of the wall and in turn the anchor force required.

## 2.4 Lateral Support of Retaining Wall

When the depth is to great the retaining walls needs horizontal support to ensure its stability. The most common way to do this is by using tie-back anchors or struts to support the wall. Anchors are drilled into the surrounding soil or rock and then anchored into the retaining wall. The anchor carry the tensile force to capable soil which can be resisted by the shear strength of the adjacent soil (Civil Engineering Oraganization, 2016). Depending on the type of lateral support used in the excavation, it's also important to ensure that there is enough room for machinery. For an example, struts attached inside the shaft obstruct space for machinery and other excavation work.

### 2.4.1 Types of Anchors

Anchors are often separated with two different types. They are either anchored in soil or rock. The choice of method depends on what the surrounding soil consists of, as well as, the distance to solid rock. The anchor can be devided into three parts: the drilled part, the free length and the locked section (Keller Grundläggning, n.d.). The free length is between the anchor nut and the concrete casted section.

The earth anchor, (2) in Figure 2.7, is drilled with a drill bit into the ground until the requested design length has been reached. In order for the anchor to be adhered to the ground, a cement mixture is injected at the same time as the drill rotates to create a texture with air pockets where the mixture can adhere to nearby soil (Hercules Grundläggning, 2022).

Generally the rock anchor, (3) in Figure 2.7, is drilled into the solid rock to a depth of 3-5m and then adhered with injection of cement mixture. Rock anchors are often preferred as it is easier to achieve the right strength when adhering to rock than it is in soil (Hercules Grundläggning, 2022).

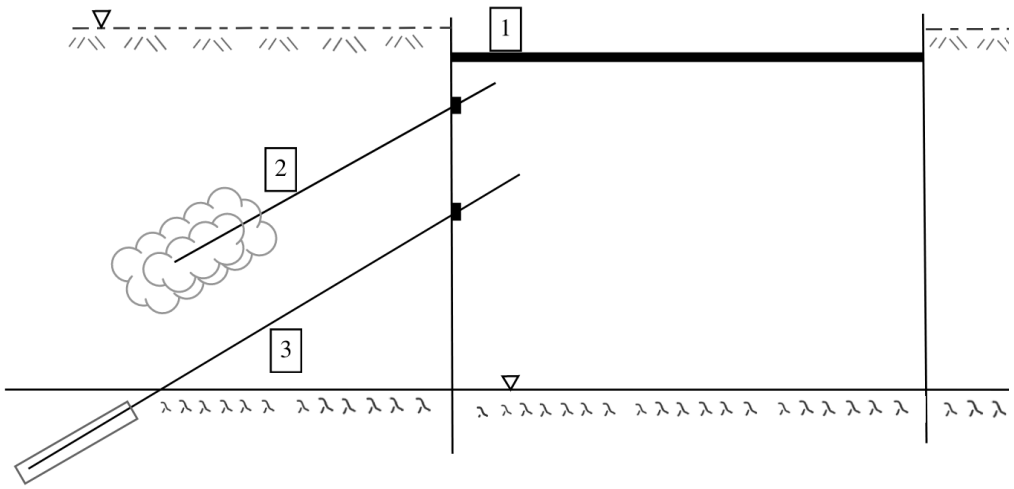


**Figure 2.7:** An illustration of a strut (1), as well as how anchors are anchored in soil (2) respectively rock (3).

### 2.4.2 Drilling Methods

The method when the anchors are drilled is often referred to as self-drilling anchors or pre-drilled anchors. The choice of method depends on the magnitude of the loads, conditions on the ground and financial aspects. Each drilling method can be useful for different cases.

The pre-drilled method is used when anchoring in rock. First, a hollow pipe is drilled until rock is reached. Secondly, a hole with a smaller dimension is created in the rock. The anchoring is made of layers of strands. Depending on what strength needs to be achieved, many strands can be intertwined into one unit. When the anchor is in place, the cement mixture is pumped into the pipe and the strands are adhered to the solid rock. Pre-drilled anchors are often used when larger forces take place in the excavation as they can be customised and have more potential than self-drilling anchors (Brattberg, 2011).

Self-drilling anchors are frequently used when grouting takes place in the soil. Unlike pre-drilled anchors, the process is completed in one step, and the anchors are frequently left behind once the construction has been completed. The system consists of a drill bit and hollow steel bars with coupling nuts. Compared to the pre-drilled anchor, the drill

bit is sacrificed in the hole. When the anchor is drilled into the soil, a cement mixture is pumped through the hollow steel bar and adheres to the soil from small holes in the drill bit.

After the cement mixture is injected and the anchor is positioned the mixture need to have a hardening time that normally is seven days (Brattberg, 2011). The time can vary depending on the properties of the cement.

### 2.4.3 Load Testing of Anchor

When the anchor is in place, a load test needs to be performed in order to ensure that the correct strength capacity is achieved. The test of capacity needs to reach a load of 80 % of the failure load and take place for a minimum of 6 loading cycles (Swedish Standards Institute, 2016). After each loading cycle, the creep deformations need to be measured over a certain period of time. The measurement will take place until the speed of creep is constant. When the load test is completed and no deviating or incorrect measured values have arisen, the anchor is stressed to the dimensional lock off load.

When the hydraulic cylinder is removed and the nut or the wedges are tightened, some reduction in load and strain is known to happen. This is due to some movement in the interlocking section and it is not preventable. During normal anchor load testing, this is noted by measuring the strain in the anchor, but can also be measured through the load cell. Based on empirical studies, this difference in strain in the anchor is for a self-drilled anchor of approximately 3 mm and for pre-drilled anchors with wedges approximately 6 mm. By pre-loading the anchor more than the lock-off load, the load loss can be accounted for in advance. This is important in order to ensure that the anchors are locked at pre-described loads.

## 2.5 Numerical Analysis in Geotechnics

When it comes to calculating and dimensioning structures, the use of the Finite Element Method, FEM, in geotechnical engineering is advantageous. FEM is frequently used to simulate complex geometries, isotropic and anisotropic materials, and a number of other materials under a variety of situations. It's also appropriate when designing a complicated structure that interacts with the soil and has to account for soil behaviour. A challenge for calculating structures in soil involves the great variety of soil properties and different behavior mechanisms for various types of soil (Popa & Batali, 2010). To address this, numerical models such as PLAXIS 2D use a variety of material models with varying input-parameter requirements, the studied models are presented in Section 2.5.1.

The finite element method can solve and approximate boundary value problems such as advanced geotechnical models. By creating a model with a finite number of elements connected to nodes, the approximated displacement of each node can be calculated. A spring can be used to demonstrate a one-dimensional finite method problem, where $k$ is the stiffness of the spring, $u$ is the displacement, and $P$ is an added force. As seen in Figure 2.8, a single spring has two degrees of freedom, one at each node (marked in

Figure 2.9). The two dimensional problem implies a spring system, seen in Figure 2.9, with three dimensions of freedom.

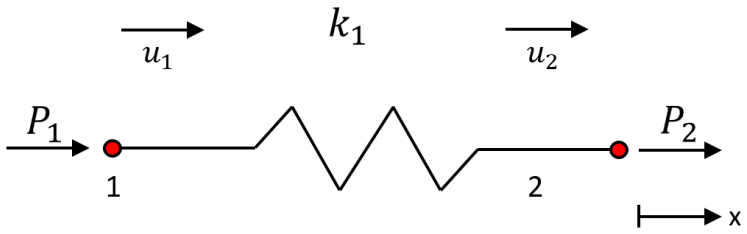


**Figure 2.8:** A single spring element with a stiffness,k, two added forces, P, and two degree of freedom, u.

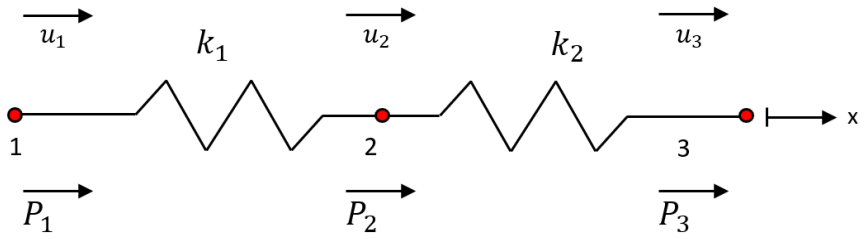


**Figure 2.9:** A spring system with two spring elements with two spring stiffness, $k_1$ and $k_2$, with three degrees of freedom.

Based on the spring Equation, 2.11, a global stiffness matrix can be extended through matrices to be valid for the whole system as 2.12. The global stiffness matrix is a more complex system including the whole system, where one more row is inserted for each added degree of freedom. The global matrices describes the whole system and not just the behaviour of individual springs.

$$ku_1 - ku_2 = P_1 - ku_1 + ku_2 = P_2 \tag{2.11}$$

$$\begin{bmatrix} k_1 & -k_1 & 0 \\ -k_1 & k_1 + k_2 & -k_2 \\ 0 & -k_2 & k_2 \end{bmatrix} \begin{Bmatrix} u_1 \\ u_2 \\ u_3 \end{Bmatrix} = \begin{Bmatrix} P_1 \\ P_2 \\ P_3 \end{Bmatrix} \tag{2.12}$$

Several material theories can be used to model numerical challenges in geotechnics, but the Mohr-Coulomb material model is the most extensively used and is also the most consistent for FEM software (Popa & Batali, 2010). Today, a wide range of software is accessible, and with faster computers, FEM simulations have evolved, implying that the issue is more with identifying parameters and selecting the proper circumstances than with generating the model.

### 2.5.1 Material models

In order to find a suitable model that simulates the soil in the most reality-like way, it is appropriate to evaluate the used material model. The models have a variation in accuracy and sensitivity depending on the type of soil and the available input parameters. Two different models are used for this study and are described in the following sections below.

#### 2.5.1.1 Mohr-Coulomb

The Mohr-Coulomb model (MC-model) can be used as a first approximation when analyzing the simulation due to it's simplicity (Bentley Systems, 2021). The Mohr-coulomb material model is an elastic perfectly plastic model where Hooke's law can relate the stress rate to the elastic strain rate, see Figure 2.10. The elastic part, ($\epsilon^e$) is linear and is influenced by the Young's modulus ($E$) and the Poisson's ratio ($\nu$). The plastic part ($\epsilon^p$) is linear and is described by the cohesion ($c$), friction angle ($\varphi$) and the dilatancy angle ($\psi$) (Bentley Systems, 2021).

The MC-model does not enable strain softening which makes it inappropriate for modelling soft soil behaviour where the mobilized shear strength often is degraded. Although, it is considered to be sufficient for preliminary results of very over-consolidated clay's, sand and rock. It is when the stress level reaches higher than the elastic stress that perfectly plastic deformations mobilizes, see Figure 2.10, which is defined by the Mohr-Coulomb failure criterion. Furthermore, it is assumed that no dilatancy occur until failure is fully mobilized.

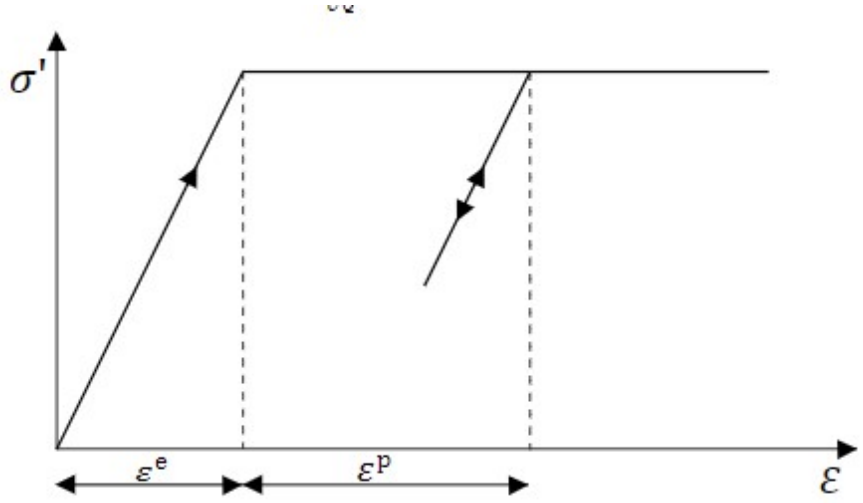


**Figure 2.10:** Perfectly plastic model. (Bentley Systems, 2021).

#### 2.5.1.2 Hardening Soil Model

The main difference, compared to the MC-model, is the definition of soil stiffness during loading/unloading and behaviour of stress-strain before non-linear failure.

For the Hardening Soil Model (HS-model) the plasticity yield surface can expand due to plastic straining (Bentley Systems, 2021). Firstly, the model uses the theory of plasticity

rather than elasticity and secondly it considers the dilatancy angle. In the HS-model the end of dilatancy that occurs when the material reaches critical state can be modelled through *Dilatancy cut-off*.

The input parameters describing the failure consist of the Mohr - Coulomb failure criteria parameters: c, $\phi$ and $\psi$. Because the model assumes plastic straining the secant modulus, $E_{50}^{ref}$, are used as a input parameter for the deviatoric loading based on a triaxial test, see Figure 2.11. Based on oedometer tests the modulus, $E_{oed}^{ref}$, can be used to explain compression. For the elastic unloading/reloading the $E_{ur}^{ref}$ (see Figure 2.11) and $\nu_{ur}$ are used as input parameters (Bentley Systems, 2021).

Compared to the MC-material model, the HS-model allows for non-linear stress-dependent stiffness and different stiffness for unloading/reloading. Furthermore, the HS-model consider volumetric and deviatoric hardening which the MC-model does not (Karstunen & Amavasai, 2017). Lastly, the HS-model take dilatancy into account before failure is reached.

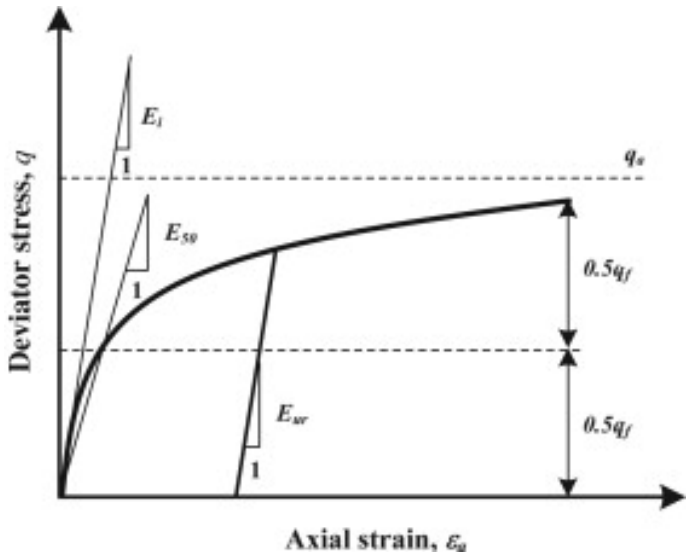


**Figure 2.11:** Principal graph of different stiffness modulus used for the hardening Soil Model related to deviatoric stress against strain. (Surarak et al., 2012).

Depending on the drainage type the parameters can be given as effective or total. Beyond the *drained* soil behaviour there are three undrained types: *Undrained A*, *Undrained B* and *Undrained C*. For the drained model and the *Undrained A* the calculations are done with effective stresses and the cohesion is combined with the friction angle, while for the *Undrained B/C* the friction angle is set to zero.

## 2.6 Similar Studies

Similar studies to this thesis have been conducted by other authors where the measured anchors force are compared to the analytically calculated ones. In the thesis *Spontberäkning Norra Länken NL51* by Jakobsson & Romero (2010) the anchor forces were compared for a sheet pile wall installed in clayey/sandy soil. The wall was supported in three levels with self-drilled anchors into rock. The measurements performed on site were conducted by ACL's and inclinometers and were compared with PLAXIS 2D and analytical calculations. Based on the results of the different calculation methods shows a significant difference between the analytical and the numerical analysis. For the upper anchors the analytical calculations showed lower values than PLAXIS although the measured values were even lower. For the lower anchors the measured value were still the lowest but PLAXIS were closer than the analytical values. In the discussion the authors conclude that the analytical and numerical analysis (through PLAXIS) was to some extent similar but the measured values varied substantially.

In the paper *Linear analysis of the anchor- ground- wall system* by Popescu & Ionescu (1978) the dependency of parameters such as, wall flexibility, anchor stiffness and stress condition in the soil on the anchor force was investigated. The paper concludes that the wall flexibility and anchor yield are of great importance for the measured anchor force. A more flexible wall indicates a higher anchor reaction and a greater anchor yield implies a lower anchor force reaction. It is also noted that a stiff anchor is not as influenced by the wall flexibility as a more flexible anchor.

In the article *Examination of the behavior of the single anchored sheet piles in sand utilizing analytical and numerical methods* by Akan (2012) differences between analytical calculations and finite element calculations are analyzed and how different parameters influence the results for a singled anchored retaining wall in sand. The retaining wall is modelled through two different methods, fixed earth theory and free end theory. Fixed end theory infer that the wall works like a beam that is assumed sufficiently embedded so that rotation is prevented. Therefore, the beam is exposed to bending moments. The results show that for the fixed end wall the maximum moment is lower than for the free end wall although the displacement is larger. The article concludes that an increased friction angle and a high anchor level decreases the anchor force. Furthermore, it can be stated that the fixed end calculation method correspond better to the finite element calculations than the free end method although all analytical results where higher in general.

# 3
# Case Description

The calculations and measurements in this thesis are conducted for a construction site in central Gothenburg. The project are further explained and the studied sections geometry and geology are presented in this section.

## 3.1 Project Hamnbanan

The port of Gothenburg is the largest port in Sweden and to handle the future increased quantities of goods expansion of the transport connections to and from the port is required. The railway through Gothenburg city is called *Hamnbanan* and has up until present day been a single-track railway. The new construction is a new permanent line with two tracks which will increase the capacity. Furthermore, today *Hamnbanan* is located above ground and acts as a barrier between different districts, which leads to deterioration of the development in the area. Then, by converting the route into a tunnel, this will allow the land to be used by the city in a better, safer and more efficient way (Trafikverket, 2015).

Skanska Sverige AB has been commissioned by the Swedish Transport Administration to carry out the construction of one part of Hamnbanan called Eriksberg - Pölsebo which mainly will be built as a tunnel. The railway will be performed as a tunnel in both solid rock and in soil through the "cut and cover" method. The soil will mainly consist of clay but in the specific part studied in this thesis it will be constructed in a layer of friction material. The studied section in this thesis is located at the east side of the project, see Figure 3.1.

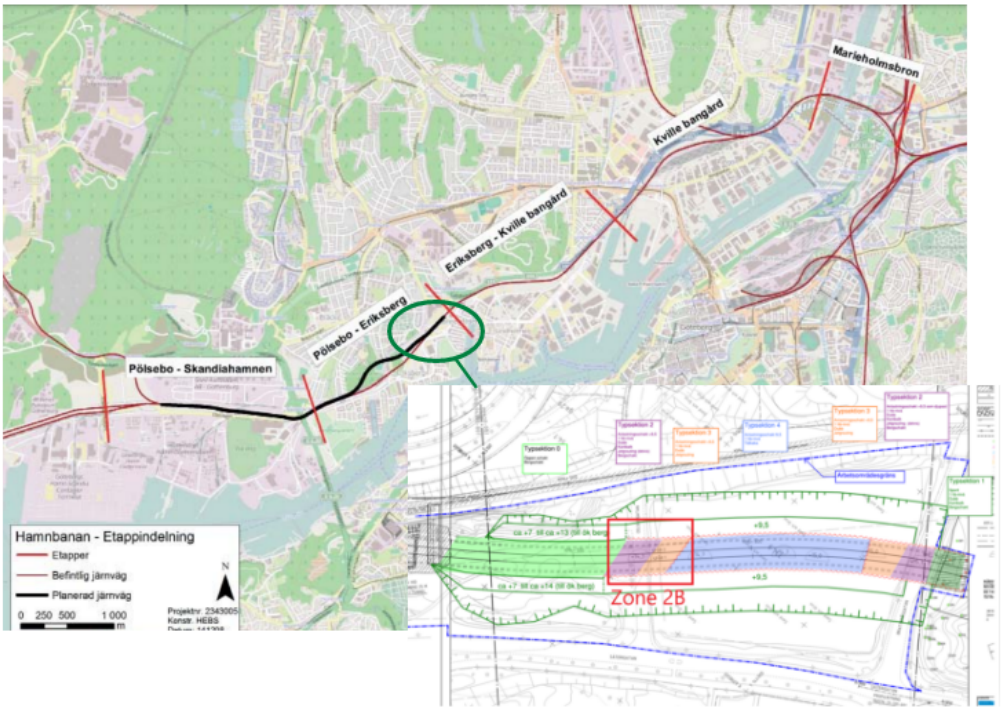


**Figure 3.1:** Profile of the studied section. (Skanska, 2020).

## 3.2 Geometry and Geology of Studied Section

The studied section is an open excavation conducted to a depth of about 7 meters. The soil depth is around 11 metres on the west side of the excavation area, and the rock surface is increasing to the east. As a result, the rock surface is above the excavation bottom on the east side, see Figure 3.2. Therefore, rock has to be removed through blasting inside the excavation for the east section. The section will then follow as tunnel in rock to the east.

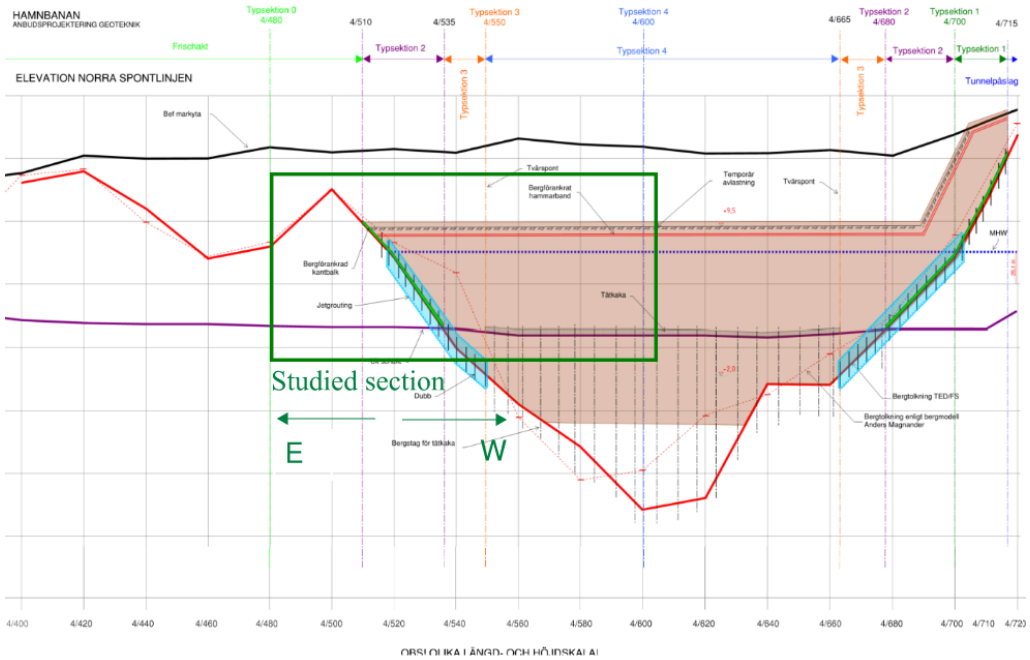


**Figure 3.2:** Cross-section of the studied area. The studied excavation is located in the displayed green rectangle. The cardinal directions are also displayed in green (Skanska, 2020).

A slope is built with an inclination of 2:1 ending about one meter from the retaining wall. For the calculations the slope is assumed to end at the retaining wall. At the top of the slope, on both sides, construction roads are located which needs to be considered.

Soil parameters for the area were evaluated based on ram sounding tests (Hfa) and cone penetration tests (CPT). The soil between the two rock levels, seen in Figure 3.2, consists of checkered sand and two main layers of silt. The top layer is relatively sorted silty sand while the bottom one contains more gravel and unsorted material. The friction angle and the Young's modulus of the sand is derived based on Hfa and CPT according to recommendations from the Swedish transport administration, TR Geo 13 (Trafikverket, 2016). The values for the soil parameters can be found in Table 3.1. The rock mass in the examined region is acid magmatic rock, which is comparable to granite in it's formation and composition and is common in the area.

**Table 3.1:** Soil parameters for the studied section

| Parameter | Value | Unit |
|---|---|---|
| $\rho'$ | 36 | $^\circ$ |
| $\gamma_{sat}$ | 18 | kN/m$^3$ |
| $\gamma_{unsat}$ | 11 | kN/m$^3$ |

The groundwater levels, GW T50$_{min}$, GW$_{medel}$ & GW T50$_{max}$, are evaluated based on a number of observation tubes in the area. All values for the groundwater levels are

presented in Table 3.2, given as meter above sea level. For all sections of the retaining wall the $HW_{dim}$ is used thus it provides the largest load effect. The wall is assumed to be free from seapage due to sealing methods and the interlocking method of the drilled piles.

**Table 3.2:** Design levels of groundwater.

| GW $T50_{min}$ | $GW_{medel}$ | GW $T50_{max}$ | $HW_{dim}$ | $LW_{dim}$ |
|---|---|---|---|---|
| 6.30 | 6.80 | 7.30 | 7.38 | 6.22 |

### 3.2.1 Design of Retaining structures

Similarly to the rest of the project the retaining walls for the studied section was designed with sheet pile walls. Thus, due to complications with gravel during installation, the method was changed to a drilled interlocking pile wall. The wall is retained, with 76 mm wide self-drilling anchors fixed in bedrock, which can be seen in Figure 3.3. The piles are drilled about one meter into the rock while the anchors are drilled five meters, which is longer than the standards. The chosen method of retaining walls and anchors implies that both retaining walls (on the north and the south side) can be seen as independent structures.

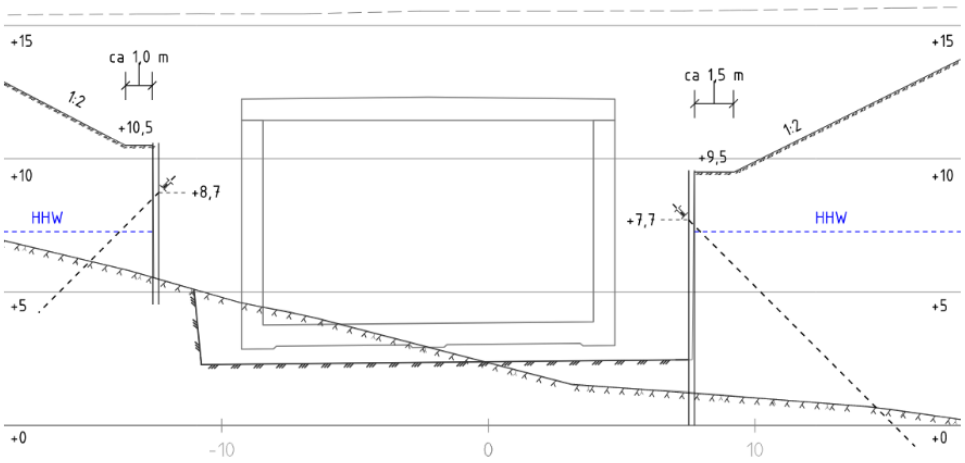


**Figure 3.3:** Section of temporary constructions and tunnel (Skanska, 2020).

The anchors are drilled with an angle of 45 degrees hence the wailing beam has the same inclination, a detailed illustration of the anchor and wailing beam can be seen in Figure 3.4.

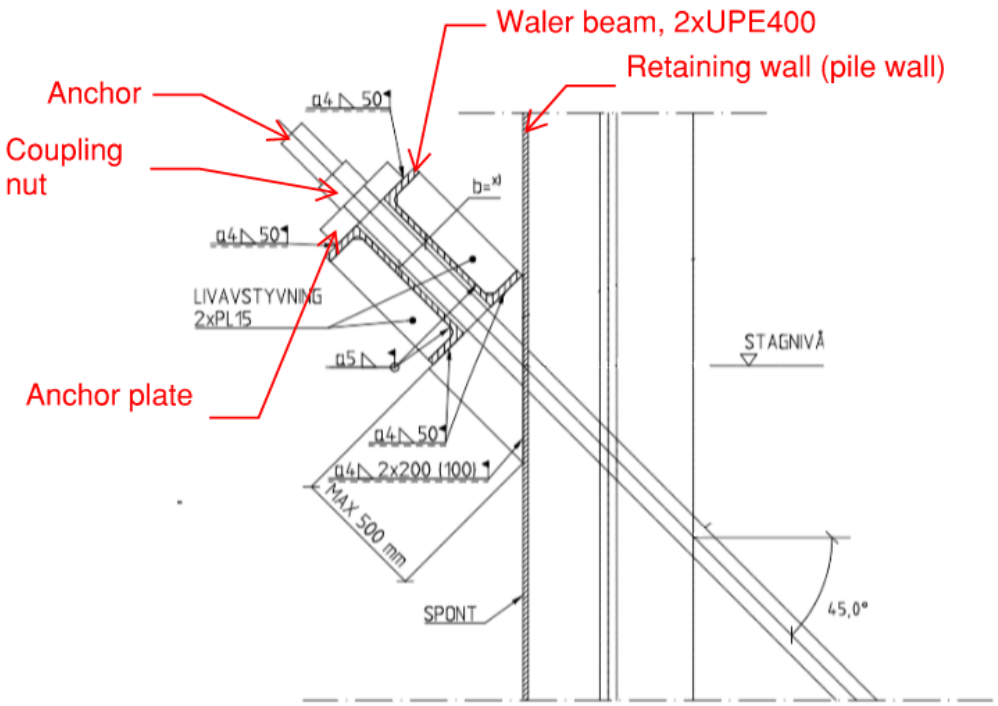


**Figure 3.4:** Detailed design of anchor and wailing beam. (Skanska AB, n.d.).

The anchors used in this design are of the model ANP 76 which is a self-drilled threaded bar. The material parameters and properties are described in Table 3.3 where the $f_{yk}$ and $f_{uk}$ is the characteristic yield and tensile stress capacity, respectively. $F_{t,Rd}$ is the capacity of tensile strength.

**Table 3.3:** Material parameters for ANP76 (ANP - SYSTEMS GmbH, 2018).

| ANP 76 | | |
|---|---|---|
| E | 210 | $GPa$ |
| G | 81 | $GPa$ |
| $A_s$ | 2620 | $mm^2$ |
| $f_{yk}$ | 460 | $MPa$ |
| $f_{uk}$ | 530 | $MPa$ |
| $F_{t,Rd}$ | 1507 | $kN$ |

The wall is of the model RD320 and is manufactured by the steel producer *SSAB* and is a hollow steel pile used for retaining walls. The dimensions of the pile are 323.9 mm and it has a thickness of 10 mm. Sheet pile walls were originally planned for the section but was exchanged to the drilled pile wall due to challenging conditions and difficulties to drive the sheet piles. The material properties for the RD320 wall are described in Table 3.4.

**Table 3.4:** Material parameters for RD320 (SSAB AB, 2022).

| RD320 | | |
|---|---|---|
| E | 210 | $GPa$ |
| $A_s^{wall}$ | 98,61 | $cm^2$ |
| $I_x$ | 12158.3 | $cm^4$ |
| EI | 25533 | $kNm^2$ |

# 4
# Methods

In the following section the methodology for analytical calculations, numerical modelling and measurements on site are presented and reviewed. Furthermore, input parameters and assumptions are displayed and accounted for.

## 4.1 Analytical Calculations

In order to perform an adequate analysis, it is according to *Sponthandboken* (Fredriksson et al., 2018) (Fredriksson et.al) appropriate to first perform an analytical calculation. The iterative process is initiated by calculating the retaining wall length based on stability against rotation, without support. For the studied sections, see Figure 3.3, the wall is drilled into rock and is thereby stable against rotation. The sectional forces in the retaining wall when supported at one level are then calculated using equilibrium, assuming that material parameters of the retaining system are not affected.

As stated in Eurocode 7 - geotechnical design (Swedish Standard Institute, 2022), the calculations should be conducted for both ULS and SLS. ULS assumes large deformations and fully mobilized soil strength, whereas the SLS assumes usage load and represents the actual load case on site. For this report ULS is calculated by using the partial coefficient method, see Chapter 4.1.4. The failure can occur in either the soil, in the structure or in both. To ensure a sufficient safety in SLS a model factor is usually added, this is however not done in this thesis thus the calculations are done to evaluate measured values and not to design the retaining system.

### 4.1.1 Acting Pressures

Before installation of anchors the retaining wall behaves like a cantilever beam. At this stage the system is statically undetermined and the wall needs to be driven to a depth where the wall is stable against rotation. This entails that the passive pressure acting on the wall is sufficient enough to solely resist the active pressure. This depth can be until bedrock or to a certain depth in the soil. Since the wall in this project is drilled into rock this stage is not deemed critical.

The stress in the soil is evaluated and calculated as described in Section 2.1. As seen in Figure 3.3 there is a slope ending at the top of the retaining wall, creating an additional driving load acting on the wall. This is accounted for as described in Section 2.2.1. Using Figure 2.3 the earth coefficients $K_a$ and $K_p$ are chosen, see Figure C.1 and Table C.1 in Appendix for the chosen values.

The net pressure acting on the wall is the sum of the active and the passive earth pressures respectively. The total acting pressure on the wall can be described with the $P_{netto}$, see 4.1.

$$P_{netto} = P_A - P_P \tag{4.1}$$

Where the input parameters for $P_A$ and $P_P$ is multiplied with partial coefficients for the ULS calculation, see Section 4.1.4. As earlier stated, the wall for this project is drilled into solid rock. For some of the sections the rock surface is at the excavation level or above it which means that no passive pressure is developed in these sections.

### 4.1.2 Retained at One Level

When the wall is retained at one level it can be unstable against rotation where the support-level becomes the rotational point. This is controlled by ensuring that the pressure acting on the wall can be obtained without failure occurring in the soil (Fredriksson et al., 2018). The stability is calculated based on horizontal and moment equilibrium. The wall is laterally supported through a waler beam and strut/anchors, see Figure 4.1. For a section where both active and passive earth pressure is established the net earth pressure will be similar to Figure 4.1 where the acting pressure with associated length is displayed.

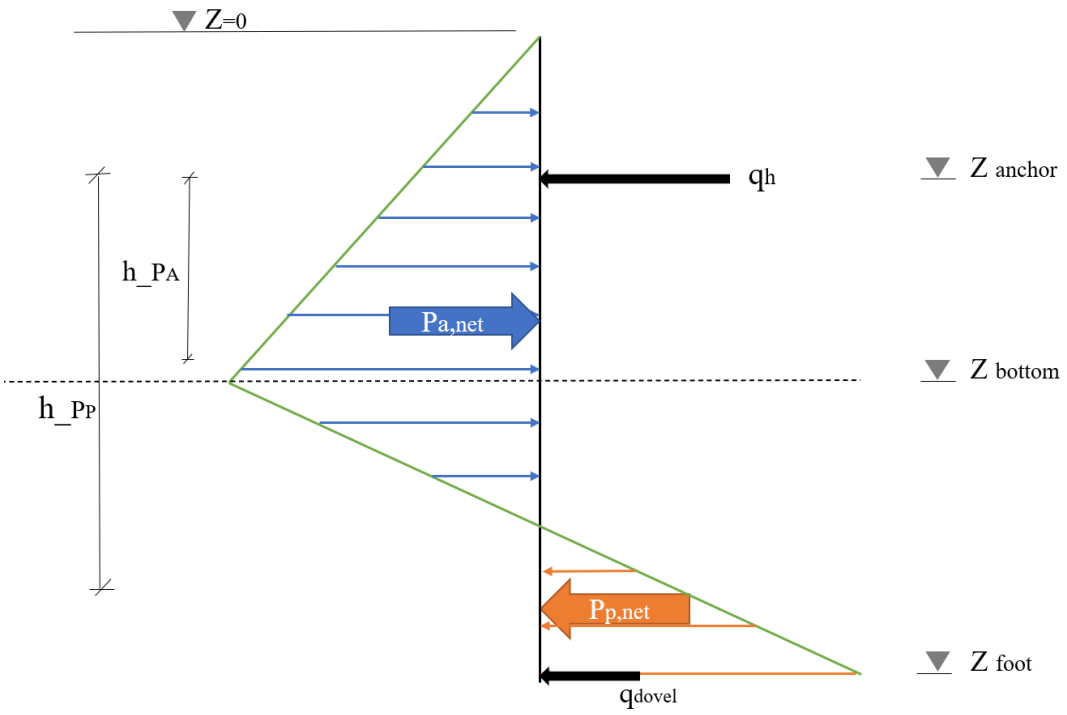


**Figure 4.1:** Principal sketch of net earth pressures acting on the wall along with depths of anchor, excavation bottom and foot of the wall. Also, the level arm for the active and passive net earth pressures are displayed.

The wall is initially calculated as a free end supported wall. The fixed end calculation method can be seen in Section 4.1.3. The free end theory is the most commonly used method and utilize active and passive earth pressure to determine the failure condition.

The rotational moment around the waler beam point, $M_q$, can be calculated as the horizontal pressure multiplied with the lever arm length, in relation to the anchor level (see Figure 4.1). This is calculated using Equation 4.2. For a free end supported wall the moment should be zero at the foot.

$$M_q = \Sigma P_{a,net} \cdot h_{Pa} - \Sigma P_{p,net} \cdot h_{Pp} \tag{4.2}$$

Since an drilled pile wall is installed for the studied retaining wall, there was no need for a rock dovel. Although, the drilled section will assimilates force and can be calculated as a rock dovel. The rock dovel force is the remaining force to ensure that the system is in equilibrium. It can therefore be calculated as the moment divided by the length between the excavation bottom and the level of the anchor, see Equation 4.3.

$$q_{dovel} = \frac{\Sigma M_q}{z_{anchor} - z_{bottom}} \tag{4.3}$$

The horizontal support required by the waler beam can be described through the horizontal force equilibrium and thereby the summarized net pressure minus the dovel force, see Equation 4.4. For an inclined waler beam, the force in the anchor direction is calculated as Equation 4.5. As can be seen in Figure 3.4 the angle, $\beta$, of both the waler beam and the anchor for the reference project is 45 degrees.

$$q_h = \Sigma P_{net} - q_{dovel} \tag{4.4}$$

$$q_{h,45^\circ} = \frac{q_h}{cos(\beta)} \tag{4.5}$$

The shear force is calculated in Equation 4.6 as the integral of the resulting earth pressure acting on the wall. In turn, the bending moment can be calculated as the integral of the shear force, see Equation 4.7 and will have it's maximum where the shear force is zero.

$$T_{Ed} = \int_{z_{bottom}}^{z_{top}} P_{net}, dz \tag{4.6}$$

$$M_{Ed} = \int_{z_{bottom}}^{z_{top}} T, dz \tag{4.7}$$

Based on the waler beam load for each calculated section the total distributed load of the waler beam can be modelled in a beam-program. The beam is supported by the anchors who are pre-determined to only obtain tension forces. The sectional forces are extracted by the beam-program and the support reactions can be evaluated as the anchor forces.

### 4.1.3 Fixed - End Support

The retaining wall is, as mentioned, drilled into rock. Realistically the embedded part of the wall will act as a support of the pile and thereby the wall. Therefore, it could be described as having a fixed-end support or partially fixed end. A fixed end can theoretically be more realistic but it is difficult to know the rock quality after drilling without extensive rock investigations. The rigidity of the support can therefore be too optimistic for a fixed end assumption since it would reduce the moment and the waler beam force and thereby act too favourably.

Therefore, to which extent the support is acting as a fixed end needs to be considered by the designing engineer. For the reference project, and for this thesis, the fixed end calculations are not done using standard beam deflection calculation cases. Instead it is calculated as a free supported beam with an additional forced moment at the support. The forcing moment at the foot of the wall is assumed to be equal to the maximal field moment. Thereby, the moment at the foot is increased through an iterative process until it is equal to the field moment, see Figure 4.2. The waler beam force can thereafter be re-calculated according to Equation 4.8 with the new assumed moment of the fixed-end wall.

$$q_{h,fixed} = q_h - \frac{M_{fixed}}{z_{anchor} - z_{bottom}} \tag{4.8}$$

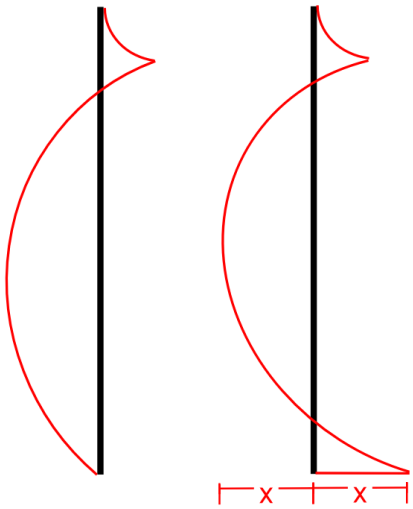


**Figure 4.2:** Principle sketch of the calculating assumption of a partially fixed end. The added forcing moment at the foot is set equal to the maximal field moment through a iterative process.

As it can be discussed how to model the partially fixed support, the assumption mentioned above is evaluated and analyzed to see how a distinction of the rigidity in the support would change the anchor force. This is done by modeling the wall as a beam with one spring support at the waler beam level and two springs at the support, see Figure 4.3 below

and E.6 in Appendix. The program, *Frame Analysis*, is used to calculate the sectional forces and the supporting forces, interpreted as the anchor forces. Since the excavation bottom is the same as the rock level no passive earth pressure is elaborated. The initial stiffness of the support is calibrated based on the original assumption described above. Thereafter it is decreased and increased by 25 / 50 and 75 percent to evaluate how the waler beam force is affected.

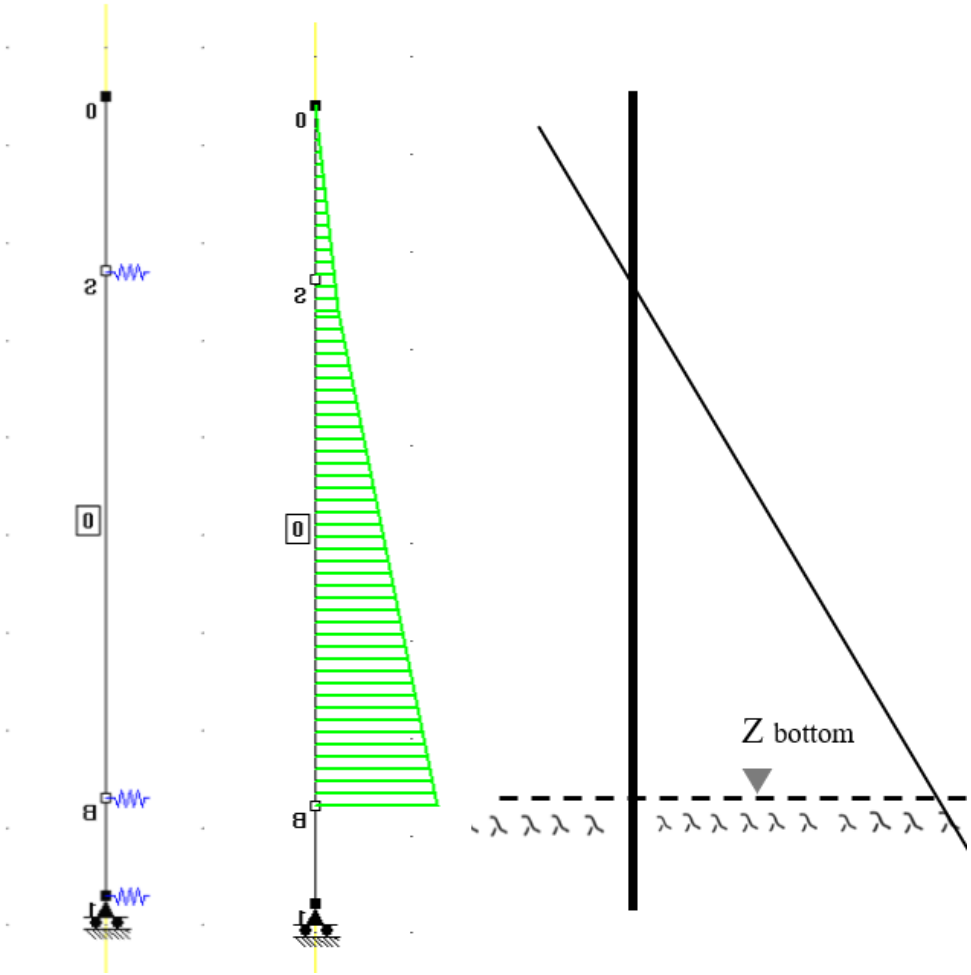


**Figure 4.3:** Setup in the beam program with two springs as support from the rock and one spring representative of the anchor. The excavation bottom and the rock surface is at the same level.

### 4.1.4 Partial Coefficient Method

The design of temporary constructions can according to Eurocode (Swedish Standard Institute, 2022) be done using the partial coefficient method to ensure a sufficient factor of safety. For the design load effect, $E_d$, the partial coefficients is applied to the load or load effect and for the design capacity, $R_d$, the coefficient is applied on the soil properties or strength (Fredriksson et al., 2018). When calculating the ULS the design values are required to be higher than the capacity:

$$E_d \leq R_d$$

The calculations at the studied project is conducted for a safety class of 2 and are calculated according to the design approach 3 (DA3) in Eurocode. For this approach the partial coefficients are applied to ground strength parameters and the influencing actions from structures (Swedish Standard Institute, 2022).

The partial coefficient for the model, $\gamma_d$, and for the material, $\gamma_M$, in the specified safety class is presented in table 4.1.4. Where $\gamma_M$ is presented for friction material, relevant for this thesis. For undrained shear strength in cohesion-less material it should be 1.5.

**Table 4.1:** Partial coefficients used for analytical calculations.

| Coefficient | Value | Description |
|---|---|---|
| $\gamma_d$ | 0.91 | Model safety class |
| $\gamma_M$ | 1.3 | Material factor |

The design values of soil properties, $\bar{X_d}$, is decided through Equation 4.9 below where $\eta$ is the conversion factor regarding the uncertainty of the model, see Table H.1 in Appendix, and $\bar{X_k}$ is the characteristic value of the studied parameter.

$$\bar{X_d} = \frac{\eta \cdot \bar{X_k}}{\gamma_M} \tag{4.9}$$

The design friction angle is modified through Equation 4.10 together with the partial coefficient for materials.

$$\tan \varphi_d = \frac{\tan_k \varphi}{\gamma_M} \tag{4.10}$$

## 4.2 2D Numerical Analysis

The software PLAXIS 2D developed by Bentley System is a finite element analysis software that can create and simulate a varies of geotechnical models in two dimensions. A variety of advanced material models based on the Mohr-Coulomb failure criterion is available in PLAXIS. This makes the software fit well with calculations and evaluation of a geotechnical issue similar to this thesis. The main purpose with the usage of PLAXIS in this report is to create a model that is as similar to reality as possible and in this way be able to compare FEM simulations against values that have been calculated analytically and the values measured in field.

The advantages of PLAXIS are that it is user-friendly with clear steps for setting up a soil model with different characteristic material parameters and the indication of the project's geometries. Its functions with analyzes and results make it easy for the user to find sources of error and adapt the model to be as similar to reality as possible.

The process for how the various steps in the finite element software were completed is shown in Table 4.2. The steps are then described in further detail in subsequent sections.

**Table 4.2:** Course of action to numerical modelling.

| **Model settings** | **Model setup** |
|---|---|
| Plane strain model<br>Element with 15 nodes<br>SI-units, gravity, water constants | Soil layers<br>Slope design<br>Cutting of excavation steps<br>Structures<br>Traffic load |
| **Properties and parameters** | **Mesh generation** |
| Defining of soil properties<br>Defining of material parameters | Creation of mesh<br>Refinement of selected areas<br>Determination of selected points |
| **Calculation phases** | **Optimization** |
| Initial phase creates earth pressure<br>Excavation steps<br>Installation of wall and anchor<br>Water flow | Refine of mesh<br>Test of reduced zone<br>Change in BC<br>Change in interface |

### 4.2.1 Model Setup

The geometry of the simulated section with descriptions of the various components can be seen in Figure 4.4. An explanation of the points in the figure are presented in the numbered list.

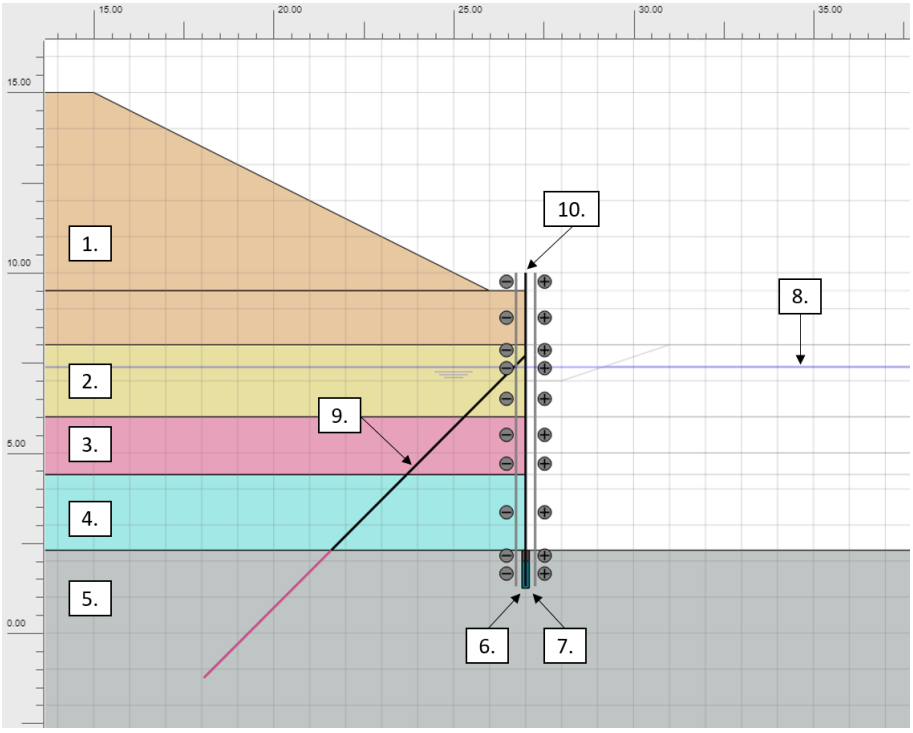


**Figure 4.4:** Model from PLAXIS with the geometry from section N2.

1. Fill material with the inclined slope. +15.0m − +8.0m.
2. Sand 1, upper section of the sand layer. +8.0m − +6.0m.
3. Sand 2, middle section of sand layer. +6.0m − +4.4m.
4. Sand 3, bottom section of sand layer. +4.4m − +2.3m.
5. Solid rock simulated as an impermeable layer. +2.3m − -$\infty$.
6. Upper layer of fractured zone where retaining wall enters the rock consisting of cement used for adhesion during installation.
7. Bottom layer of fractured zone where retaining wall enters the solid rock. The zone consists of a more brittle rock which has been created by the drilling.
8. Ground water level set to +7.38m according to site investigations performed by Skanska.
9. Retaining wall modeled as "plate" in PLAXIS, drilled 1.0m into the bedrock.
10. Anchor with inclination of 45°, modeled as "node-to-node anchors" in PLAXIS and is drilled 5.0m into the rock. The anchor is composed with the wall at +7.7m.

### 4.2.2 Input Properties and Parameters

The Hardening Soil model is used to simulate the four different soil layers, all of which consist of coarse-grained friction soil. This also means that a more realistic representation

of the simulation can be created than would have been possible with the Mohr-Coulomb model.

The input values for the soil layers are described in Table 4.3 and is a combination of evaluated values from site investigations, assumptions, and empirical values from similar studies in the area.

**Table 4.3:** Input values for soil material, PLAXIS.

| Soil values input | | | | | |
|---|---|---|---|---|---|
| Parameter | Unit | Sand 1 | Sand 2 | Sand 3 | Fill |
| $\gamma_{unsat}$ | $kN/m^3$ | 11 | 11 | 12 | 13 |
| $\gamma_{sat}$ | $kN/m^3$ | 18 | 17 | 19 | 23 |
| ${E_{50}}^{ref}$ | $kPa$ | 9,0·$10^3$ | 6,5·$10^3$ | 12,0·$10^3$ | 50,0·$10^3$ |
| ${E_{oed}}^{ref}$ | $kPa$ | 11,0·$10^3$ | 7,8·$10^3$ | 14,6·$10^3$ | 59,8·$10^3$ |
| ${E_{ur}}^{ref}$ | $kPa$ | 27,0·$10^3$ | 18,7·$10^3$ | 35,1·$10^3$ | 143,5·$10^3$ |
| $c'$ | $kPa$ | 0,2 | 0,2 | 0,2 | 0,2 |
| $m$ | - | 0,5 | 0,5 | 0,5 | 0,5 |
| $\phi'$ | $^\circ$ | 33 | 32 | 33,5 | 38 |
| $\psi$ | $^\circ$ | 3 | 2 | 3,5 | 8 |
| $k_x$ | $m/day$ | 1 | 1 | 1 | 0,086 |
| $k_y$ | $m/day$ | 1 | 1 | 1 | 0,086 |

The solid rock is simulated by the Mohr-Coulomb model with the parameters set to high strength since the goal is for the rock to function as completely solid and that the material should not have a major impact on the model in general. The zone around the crop where the sheet pile wall enters the rock is assumed to have reduced strength. In this case two materials are simulated, brittle rock and concrete they are both presented in Table 4.4.

**Table 4.4:** Input values for solid rock and reduced zone, PLAXIS.

| Solid rock and reduced zone values input | | | | |
|---|---|---|---|---|
| Parameter | Unit | Solid rock | Brittle rock | Concrete |
| $\gamma_{unsat}$ | $kN/m^3$ | 25 | 24 | 24 |
| $\gamma_{sat}$ | $kN/m^3$ | 25 | 24 | 24 |
| $E$ | $kPa$ | 60.0 ·$10^6$ | 3.5 ·$10^6$ | 25.0 ·$10^3$ |
| $c_{ref}$ | $kPa$ | 4000 | 2000 | 400 |
| $\nu$ | - | 0.25 | 0.24 | 0.2 |
| $\phi$ | $^\circ$ | 42 | 32 | 35 |
| $\psi$ | $^\circ$ | 12 | 12 | 5 |

The anchors are modeled with the element "node-to-node anchor" and the only input parameter required for PLAXIS is the normal stiffness hence the assumption of an elastic behavior of the anchor. The normal stiffness is calculated through Equation 4.11 with the material parameters from Table 3.3.

$$EA = E_s \cdot A_s^{anchor} \tag{4.11}$$

The input values that is necessary when modeling the anchor in PLAXIS are presented in Table 4.5.

**Table 4.5:** Input parameters for anchors, PLAXIS.

| Anchor parameter input | | |
|---|---|---|
| Parameter | Unit | Values |
| Material type | - | Elastic |
| $EA$ | $kN/m$ | 525.0 ·$10^3$ |
| Spacing | $m$ | 3.0 |

A material set for a *"plate"* is used to simulate the retaining wall. The wall is immersed into the rock where a small area of a more reduced strength material is created. Converting the parameters from Table 3.4 using Equation 4.11 for the normal stiffness and Equation 4.12 for calculating the flexural stiffness. The input values that are necessary when modeling the retaining wall in PLAXIS are presented in Table 4.6.

$$EI = E_s^{wall} \cdot I_x^{wall} \tag{4.12}$$

**Table 4.6:** Input values for sheet pile wall, PLAXIS.

| Structure values input | | |
|---|---|---|
| Parameter | Unit | Sheet pile wall |
| Material type | - | Elastic |
| $EA_1$ | $kN/m$ | 2.0·$10^6$ |
| $EI$ | $kNm^2/m$ | 65.8 ·$10^3$ |
| $w$ | $kN/m/m$ | 2.36 |
| $\nu$ | - | 0.28 |

### 4.2.3 Hydraulic Flow Conditions

The level of the groundwater surface is fixed at +7.38 m and is assumed constant in all models, according to the designing groundwater levels reported in Table 3.2. The permeability is irrelevant because the finite element program performs a plastic analysis, and because it is time-dependent, values are set to 0.001 for the software to function properly (Bentley Systems, 2021).

The conditions for water pressure in the shaft pit are also altered when each step of excavation is completed. The excavated volume is transformed to a dry cluster, and the pore pressure in the underlying layer is interpolated at the same time. This is done to ensure that the model does not have any water-related errors.

### 4.2.4 Embedded section

A zone has been created in the setup of FEM-simulations where the retaining wall is embedded into the bedrock to simulate how drilling in rock affects the strength surrounding the attachment of the retaining wall, see Figure 4.5. The zone is divided into two parts, predicated on the assumption that the upper part of the drilled zone will be weaker than the lower part. Different materials are evaluated, and a result is produced when simulation results resemble the field results.

Solid rock, fragile rock, and concrete will be tested in the simulation for the reduced strength zone. It is assumed for solid rock that no reduction in strength occurred while drilling, for brittle rock that some crack formation occurs, and for concrete that the material used for bonding between rock and retaining wall absorbs stress.

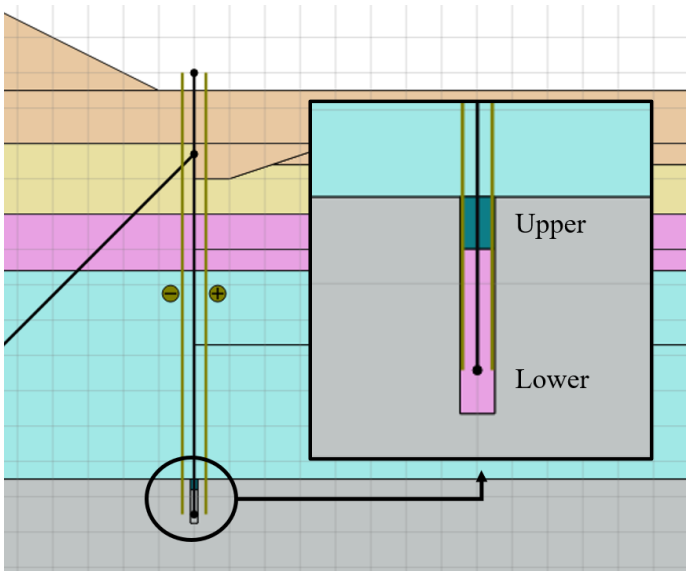


**Figure 4.5:** Zone were reduced material parameters are simulated.

### 4.2.5 Calculation Phases

The steps to simulate the installation of retaining wall and anchors with the realistic excavation steps is presented in Table 4.7. The loading type for the excavation steps is set to "stage construction". This allows for a realistic modelling of the removed soils' nonlinear, time-dependent, and anisotropic behaviour. To optimise the model, some simplifications are made with the level of excavation and times when the project was stopped and no construction work are performed.

**Table 4.7:** Calculation phases in PLAXIS.

| Phase | Event | Description |
|---|---|---|
| Initial phase | Gravity loading | - |
| 1 | Installation | Sheet pile wall driving |
| 2 | Excavation | Removal of soil to wailing beam level |
| 3 | Installation | Drilling of anchor |
| 4 | Pre-stressing | The load is applied to anchor |
| 5 | Excavation | Removal of soil to +7.0m |
| 6 | Excavation | Removal of soil to +4.0m |
| 7 | Excavation | Removal of soil to full depth |

## 4.3 Measurements On-Site

The north section can be seen in figure 4.6 and is designed with a higher number of anchors and a longer wall length. It was believed that the ALC of these anchors would not indicate any differences compared to the lock-off load. In consultation with the responsible designing engineer it was therefore decided to lower the lock-off load at the North section to provide more significant findings in measurements. Consequently four (ALC 3-6) of the six load cells where placed on the north section, while the other two (ALC 1-2) where installed on the south section for reference data. The location of the load cells can be seen in figure 4.6 below and D.1 in Appendix.

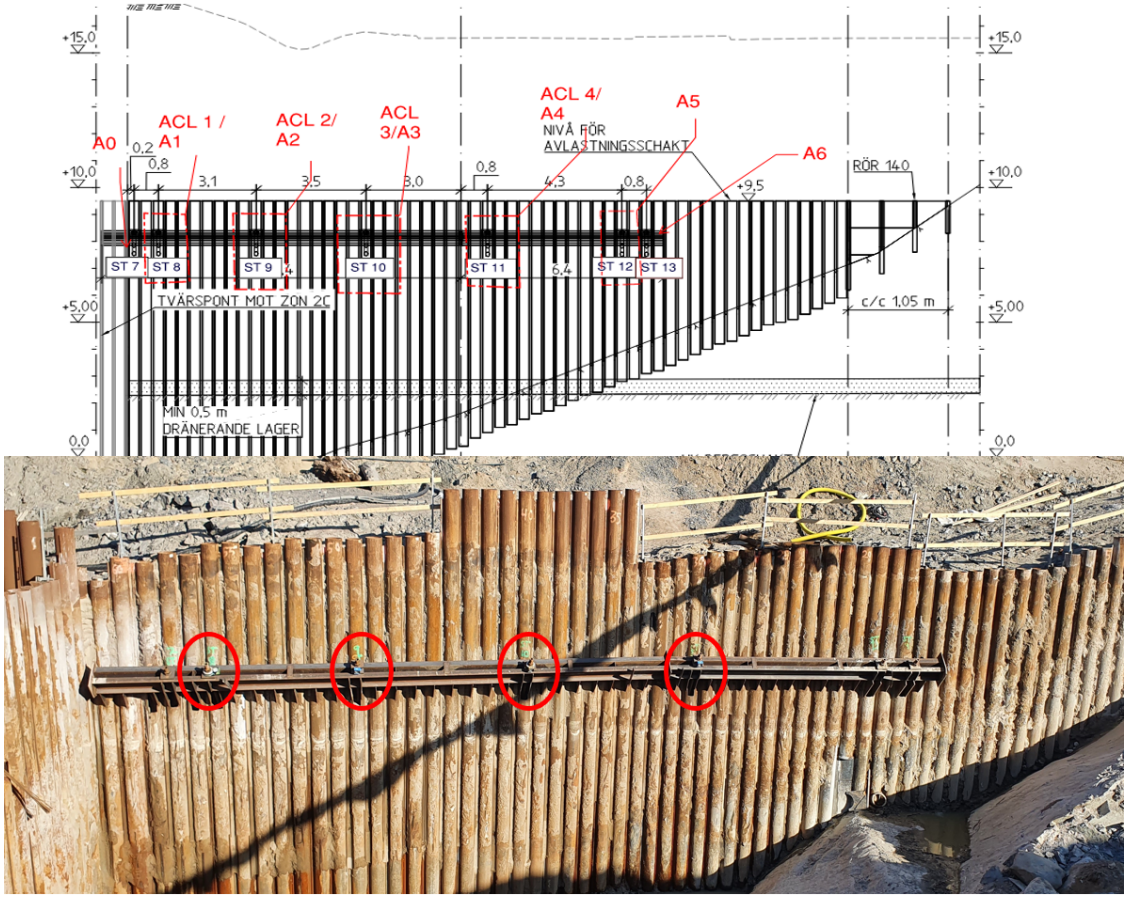


**Figure 4.6:** Locations of the load cells for the north wall.

The load cells are analog and each of them needs to be read manually. This entails that measurements for all times are not possible. The collection of data occurs everyday during the excavation process until full depth is reached. No reading takes place when work is at a standstill, such as weekends and holidays. When the full excavation depth has been reached, the data is collected every two days and at relevant events that may have an impact on the outcome, such as blasting in adjacent rocks.

As the shaft is initially shallow, the sensors can be read with the naked eye. As the excavations continue, the distance up to the ALC's becomes longer and an equipment is

needed to read a value. The solution is a tool where an optical equipment is mounted on an extendable shaft, which creates the possibility of measuring the ALC's from different heights / depths. By image processing of the optical equipment, a value can be extracted and documented.

### 4.3.1 Anchor Load Cell

The measurement of anchor forces is conducted through the installation of Anchor Load Cells (ALC) at six specific anchors in the studied project section as mentioned in section 4.3. The ALC is a measuring instrument from the German company, GLÖTZL, that manufactures different types of measuring instruments for the industry (GLÖTZL, 2019) and is where the load cells are sent for calibration before installation. The ALC's are mounted between the anchor plate and the anchor nut after the anchor have been tested with the proof-load and before the anchor is loaded to the lock-off load, see figure 4.7. It is then monitored for changes in load when excavation is performed.

**Figure 4.7:** An installed ALC, from studied site.

This specific load cell is identified as two iron-pads with ring groves in between which enables the pads to move and generate a pressure. The pressure piston is connected with a hydraulic manometer and through this solution the hydraulic pressure can be converted into a load in kilo Newton (kN). The cell provides the pressure through an hydraulic liquid and have a sensitivity of $\pm$ 1 kN/kN where the maximum load of the cell is 750 kN. The temperature range is specified to -25 ° to 80 ° (GLÖTZL, 2019).

# 5
# Results

In the following section the results for the analytical and numerical calculations as well as the measured values are presented. The results are then compared in section 5.4 which is then followed by an analyses of the utilization rate. The analytical and numerical calculations is solely done for the North retaining wall and the measured anchor forces of the south side are used as reference values, therefore only the north section results are compared with calculated ones.

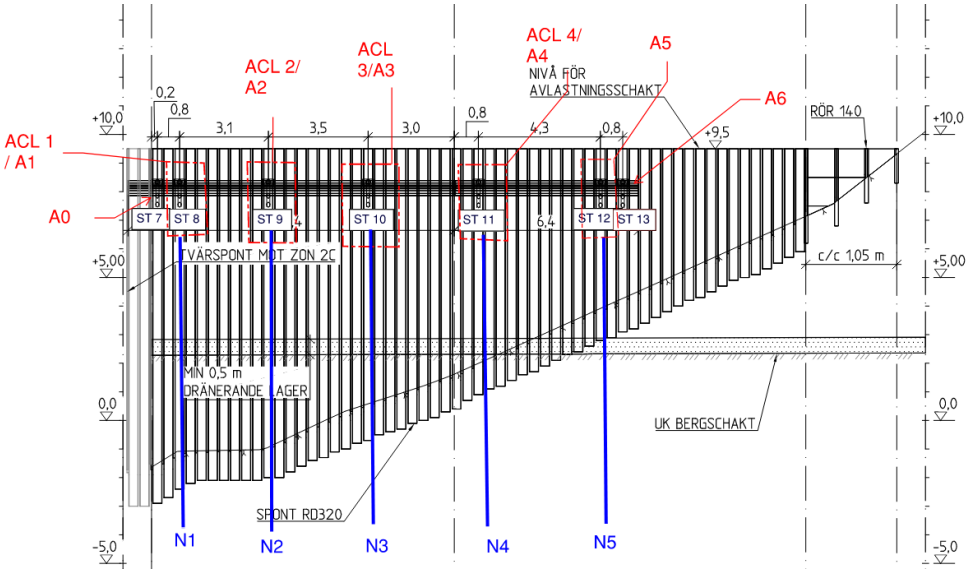


**Figure 5.1:** Allocation and numbering of anchors and anchor load cells along with the calculation sections

## 5.1 Analytical Calculations

The SLS calculation results are assumed to be representative for the analytical results as the intention of setting all partial coefficients to 1 were to retrieve realistic earth pressures. Based on the material data of the studied site, the pore water pressure along with the active and passive earth pressure can be calculated and plotted against the depth. In Figure 5.2 the earth pressures acting on the retaining wall are displayed, including the net earth pressure. The earth pressure coefficients, $K_A$ and $K_P$, which consider the adjacent slope, are included in the earth pressure. The earth pressures for the remaining sections are displayed in Appendix A.

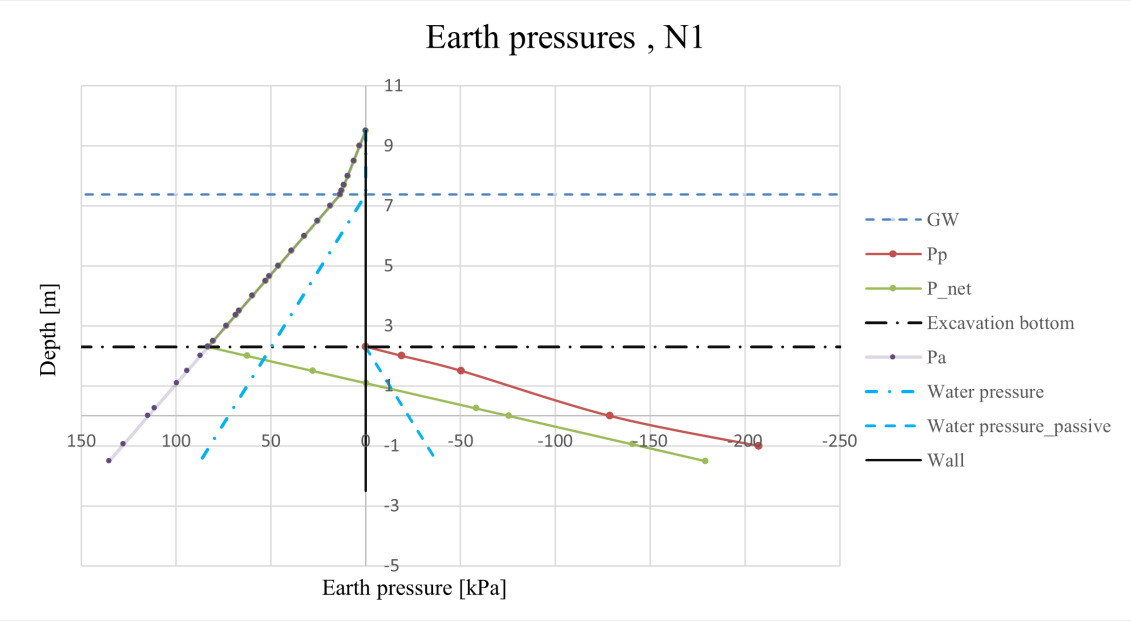


**Figure 5.2:** The pressures acting on the retaining wall for section N1.

### 5.1.1 Moment and Shear Force

The analytical shear force and bending moment in the wall are calculated as described in Section 4.1.2 and is displayed in Figure 5.3 below as well as in E.1 - E.4 in Appendix. The red graph's displays the moment, where the dashed graph represents the free end calculation. The solid graph is the reduced moment representing the assumption of an added forcing moment due to the partially fixed support of the wall. The blue graph's in the figure are the shear forces where the dashed line is for the free end calculation and and the solid line represents the partially fixed end with reduced values. It can be seen how the bending moment has the maximum value where the shear force is zero. For section N1 and N2 it can be seen that the shear force decreases to zero at the foot of the wall, while for section N3-N5 the shear force and the foot of the wall is far from zero. This depends on the excavation level and if a sufficient amount of passive pressure can be developed.

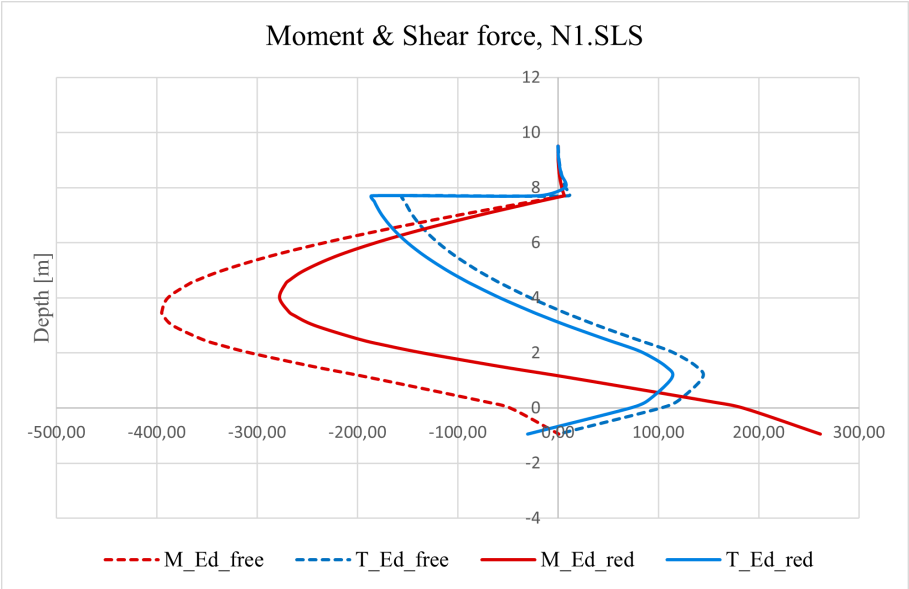


**Figure 5.3:** Moment and shear force for section N1

Table 5.1 summarize the result of the analytical calculations and the moment and shear force of the wall for the different calculated sections. All sections have different geometry since the level of the rock varies, although the anchors are in the same level, see Figure 5.1. $M_{rotation}$ is the driving rotational moment based on earth pressure.

**Table 5.1:** Moment and shear force from SLS-calculation for each calculation section.

| **Section** | $T_{max,free}$ [KN] | $T_{max,fixed}$ [KNm/m] | $M_{rotation}$ [KNm/m] | $M_{max,free}$ [KNm/m] | $M_{max,fixed}$ [KNm/m] |
|---|---|---|---|---|---|
| **N1** | 155.32 | 185.47 | 1135.69 | 394.92 | 277.36 |
| **N2** | 155.66 | 187.39 | 1135.69 | 396.38 | 272.82 |
| **N3** | 159.96 | 167.34 | 1135.69 | 328.74 | 217.77 |
| **N4** | 162.49 | 147.72 | 877.44 | 173.99 | 115.32 |
| **N5** | 61.94 | 58.68 | 198.20 | 38.71 | 25.95 |

When the wall is assumed to be fixed or partially supported, the moment of the wall can't be adjusted without accounting for the change in shear force, which is also affected. By decreasing the moment the shear force increases. The change in shear force is calculated based on the revised bending moment of the wall and is also displayed in figure 5.3. The drilled pile wall has due to it's geometry and material properties good ability to sustain shear force and the bending moment is usually more critical at an earlier stage, alternatively the moment and shear force combined.

### 5.1.2 Waler Beam Load

Based on the shear force and the rotational moment of the wall the waler beam strain can be calculated, displayed in Figure 5.4. As can be seen the waler beam force decreases as the level of the rock approaches the surface. The displayed values are based on each calculation section, seen in Figure 5.1. The waler beam of the section has an inclination of 45 degrees which has to be taken into consideration and each sections horizontal force and inclined force is displayed in Table 5.2.

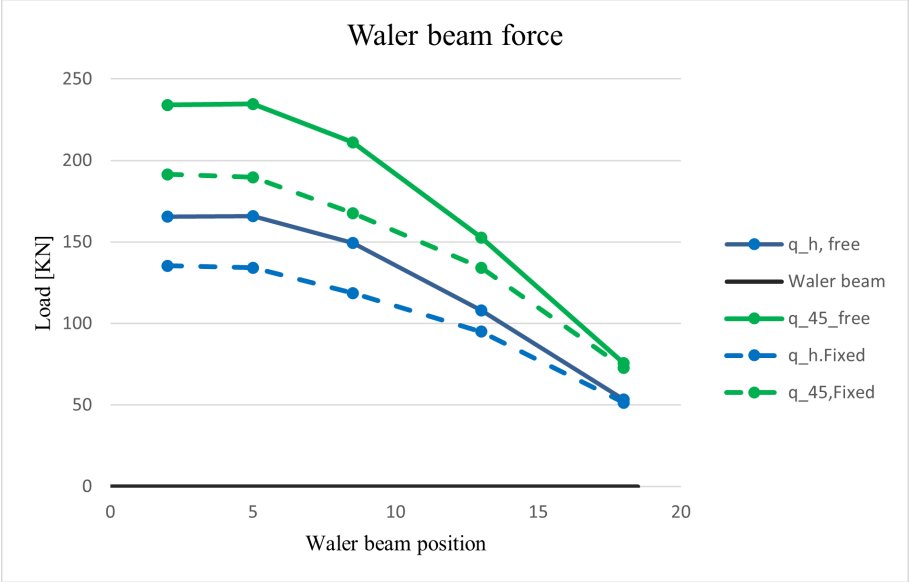


**Figure 5.4:** Force along waler beam

**Table 5.2:** The waler beam forces for section N1-N5 based on SLS calculations.

| | $\mathbf{q}_{h,freeend}$ | $\mathbf{q}_{45,freeend}$ | $\mathbf{q}_{h,fixedend}$ | $\mathbf{q}_{45,fixedend}$ |
|---|---|---|---|---|
| **N1** | 166 | 117 | 135 | 96 |
| **N2** | 166 | 117 | 134 | 95 |
| **N3** | 149 | 106 | 119 | 84 |
| **N4** | 108 | 76 | 95 | 67 |
| **N5** | 54 | 38 | 51 | 36 |

### 5.1.3 Anchor Forces

Since the length of the anchors vary, due to depth down to bedrock, the stiffness of the anchors vary as well. The setup for the beam-model and anchor force calculation is displayed in Figure 5.5.

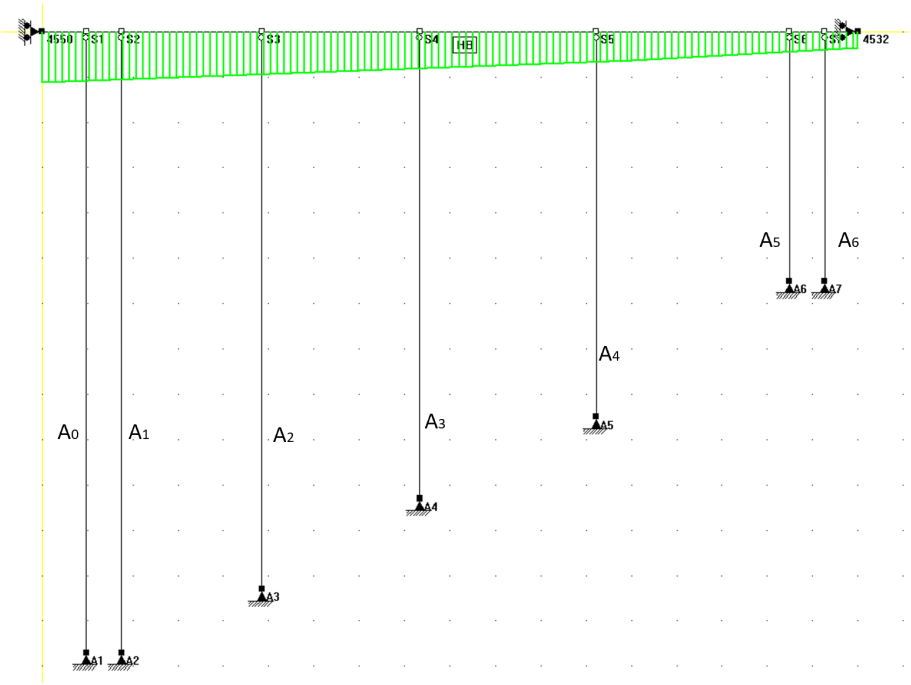


**Figure 5.5:** Set-up for the beam model, calculating the anchor forces based on waler beam load.

The respective anchor force is presented for all three limit states in Table 5.3. As expected, it can be seen that the ALS results has the highest anchor force followed by the ULS and the SLS has the lowest results. Results in Table 5.3 are valid for the fixed end assumption of the wall and are given in the anchor direction of 45 degrees. Note that ALC 0-1 had a lock off load of 210 kN, 2-4 of 360 kN and A5-6 a load of 120 kN.

**Table 5.3:** Analytical results for anchor forces in SLS, ULS and ALS. All results are for a partially fixed end support.

| **Anchor** | **SLS [kN]** | **ULS* [kN]** | **ALS*** [kN] |
|---|---|---|---|
| A0 | 301 | 380 | 670 |
| A1 | 362 | 430 | 800 |
| A2 | 575 | 715 | 1090 |
| A3 | 594 | 735 | 1155 |
| A4 | 543 | 760 | 1240 |
| A5 | 261 | 340 | 590 |
| A6 | 41 | 60 | 290 |

* Values are provided by the contractor and the design documents (Skanska Sverige AB, 2021).

### 5.1.4 Evaluation of Assumption

The analytical assumption with an additional forced moment at the foot of the wall due to a partially fixed end is evaluated by changing the moment in the foot and analysing the response in the waler beam. The spring representing the waler beam is set to resemble the anchor at a value of 22 000 kN/m. The initial stiffness in the two springs representing the rock is calibrated according to the initial assumption where the field moment is equal to the moment in the foot of the wall and is set to 230 000 kN/m.

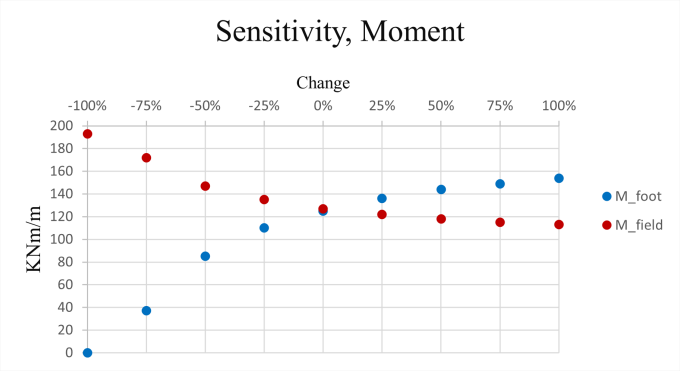


**Figure 5.6:** Change in field moment and at the foot of the wall when increasing and decreasing the stiffness of springs.

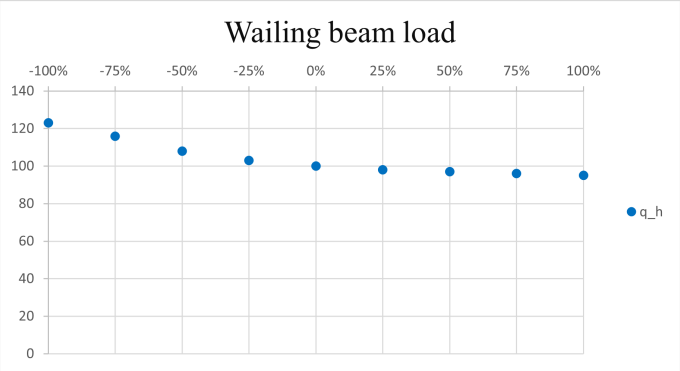


**Figure 5.7:** Change in waler beam load when increasing and decreasing the stiffness of springs.

Using the beam program the extreme values is accounted for by setting the support as totally fixed and free, as seen in Table 5.4.

**Table 5.4:** The field moment and the moment at the foot for the wall with change of rigidity for the embedded section.

| Support | $M_{field}$ [kNm/m] | $M_{foot}$ [kNm/m] | $q_h$ [kN] |
|---|---|---|---|
| Fixed | 82 | 224 | 82 |
| Free | 193 | 0 | 123 |

## 5.2 Measured Values

The value of each separate load cell can be seen in Appendix G and compiled in Figure 5.8. Note that ALC 1 is lower than the rest due to it being at the edge of the waler beam located next to another anchor at a distance of 0.8 meters, see Figure 5.1. ALC 6 and ALC 5 are located at the south retaining wall, see Figure D.1 in Appendix, while the rest of the load cells are on the north wall as shown in 5.1.

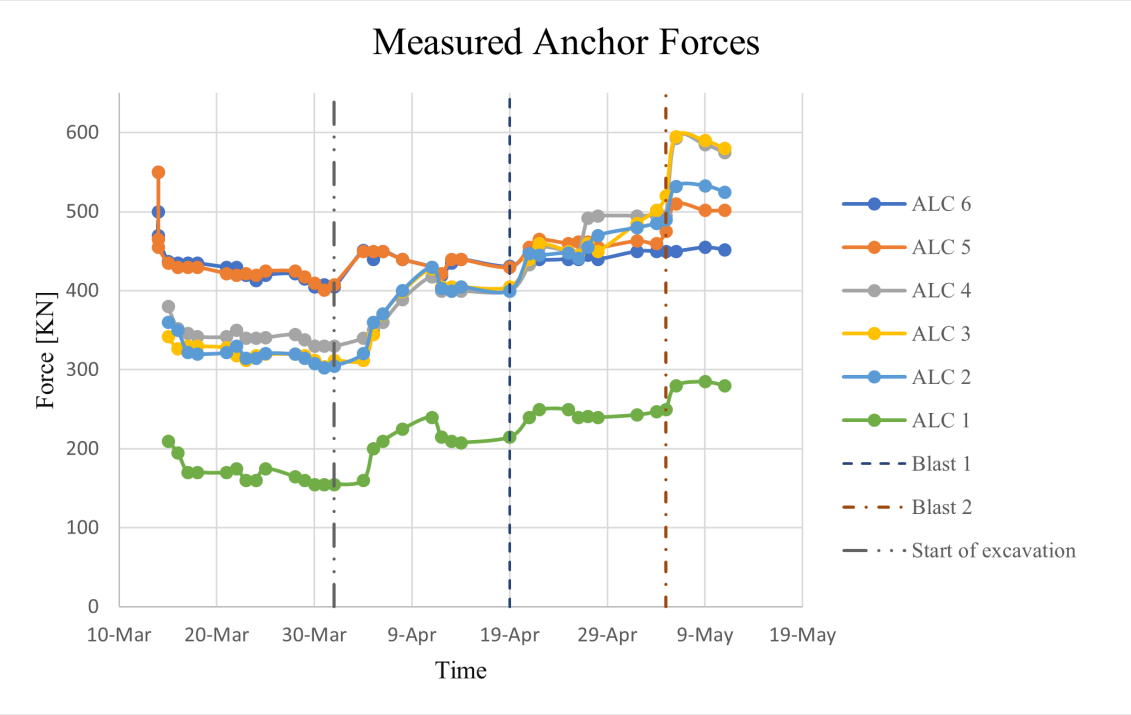


**Figure 5.8:** On-site measured anchor forces for both the north wall and the south wall.

As can be seen in Figure 5.8 the anchor forces increase with time in general but especially during excavation and blasting. The excavation started by the south retaining wall (ALC 5 and 6) which explains why ALC 5 and 6 increases earlier than the rest. Full excavation is considered to be before the second blast. The second blast generated a significant increase in anchor force which before that had stagnated. The increase in force from the blasting is not considered in the analytical calculations or the numerical-calculations. The chosen representative values for measured full excavation are presented in Table 5.5 and the increased forces due to blasting are presented in column 3.

**Table 5.5:** Chosen Anchor forces representative for full excavation and values after second blasting. A1-A4 is located on the North wall and A5-A6 on the South.

| Anchor | Chosen Value | 2nd Blasting |
|---|---|---|
| A1 | 243.5 | 281.7 |
| A2 | 470.2 | 530.0 |
| A3 | 477.0 | 588.3 |
| A4 | 486.2 | 548.3 |
| A5 | 462.8 | 504.7 |
| A6 | 445.8 | 452.3 |

### 5.2.1 Load Loss

The reduction in load which was read from ALC when mounting anchors was noticeable and the percentage reduction for each anchor is shown in Figure 5.9. It can be noticed that the direct loss in load varies from 9 to 19 % of the original lock-off load.

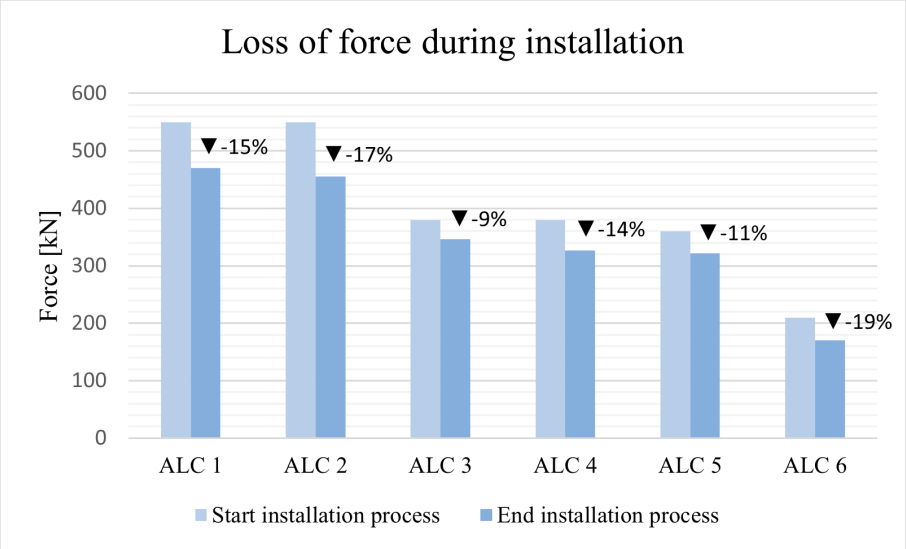


**Figure 5.9:** Loss of force during installation for anchors.

The loss of load during the installation of the anchors can be related to a loss of strain in the anchor. This depends on the free length of the anchor and anchor properties, where the latest is the same for all anchors in this reference project. The strain of the anchors in the start of the installation is defined as the load where the nut is locked and the end of installation is described as the load when the hydraulic cylinder is released and removed.

**Table 5.6:** Strain in the anchors due to the pre-stress load. The length of the anchor is the free length.

| **Anchor** | **Anchor length [m]** | **Start instal. [mm]** | **End instal. [mm]** | **Diff. [mm]** |
|---|---|---|---|---|
| A1 | 19 | 7.61 | 6.16 | 1.45 |
| A2 | 16 | 10.99 | 9.83 | 1.16 |
| A3 | 16 | 11.60 | 9.98 | 1.62 |
| A4 | 10 | 7.25 | 6.60 | 0.65 |
| A6 | 7 | 7.35 | 6.08 | 1.27 |
| A7 | 7 | 7.35 | 6.28 | 1.07 |

## 5.3 Numerical 2D simulations

The final material characteristics in the reduced strength section where the retaining wall penetrates the rock are shown in Table 5.7. Different material setups are examined, and the material that generates the same anchor forces (N) and wailing beam load ($q_h$) as the measured values and analytically calculated values are simulated.

**Table 5.7:** Determination of material properties of the reduced strength section where the wall is embedded into rock. The values marked in red indicates which material has been chosen for the drilled zone.

| | **A1** | | **A2** | | **A3** | | **A4** | |
|---|---|---|---|---|---|---|---|---|
| | N [kN] | $q_h$ [kN] | N [kN] | $q_h$ [kN] | N [kN] | $q_h$ [kN] | N [kN] | $q_h$ [kN] |
| Measured | 243 | 135 | 470 | 134 | 477 | 119 | 486 | 95 |
| SR | 222.8 | 123.0 | 420.1 | 125.2 | 465.8 | 137.5 | 436.5 | 81.1 |
| BR + SR | 245.6 | 129.0 | 433.2 | 111.8 | 469.0 | 129.3 | 442.0 | 81.1 |
| C + SR | 262.8 | 143.0 | 441.0 | 125.8 | 486.9 | 144.0 | 458.6 | 85.1 |
| BR | 262.1 | 132.3 | 430.0 | 117.2 | 462.0 | 136.3 | 442.2 | 82.3 |
| C + BR | 268.2 | 141.0 | 472.4 | 125.3 | 491.8 | 143.0 | 478.3 | 87.0 |
| C | 298.3 | 153.0 | 533.0 | 170.0 | 541.3 | 157.0 | 520.0 | 87.3 |

SR - Solid Rock, BR - Brittle Rock, C - Concrete.

The numerical analyses' final anchor forces are shown in Table 5.8. The final values are presented for the full excavation depth.

**Table 5.8:** Anchor forces from numerical analyses for full excavation depth.

| Anchor | Numerical [kN] |
|---|---|
| A1 | 245.6 |
| A2 | 472.4 |
| A3 | 469.0 |
| A4 | 478.3 |

Figure 5.10 presents the outcomes of the PLAXIS simulation with regard to anchor forces. It begins with the pre-stress of the anchors, progresses through the excavation stages, and concludes with the obtained load once the full excavation is obtained.

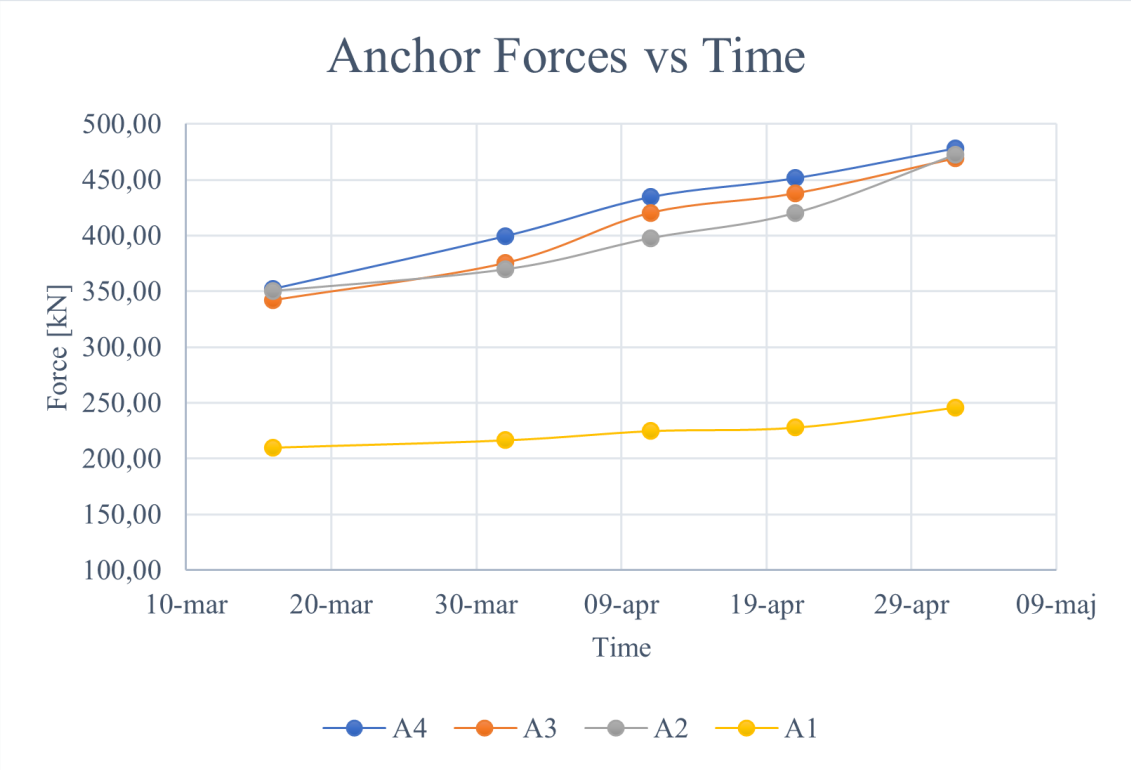


**Figure 5.10:** Anchors forces from PLAXIS

### 5.3.1 Moment and Shear Force

With regard to the compiled set of material in the drilled part, results for the moment in the retaining wall can be obtained. Results for each section from the numerical analysis are reported in Table 5.9. In Figure 5.11 it can be seen how the moment varies with the depth. The assumption that the maximum moment occurs where the retaining wall meets the rock results in the values in Table 5.9 are retrieved for this point, see Figure 5.12 for the illustration of the maximum point.

**Table 5.9:** Field moment and moment where the retaining wall meets bedrock.

| Section | $M_{field}$ [kNm/m] | $M_{foot}$ [kNm/m] |
|---|---|---|
| $N_1$ | 237.6 | 401.3 |
| $N_2$ | 130.4 | 254.2 |
| $N_3$ | 137.9 | 371.4 |
| $N_4$ | 66.8 | 201.4 |

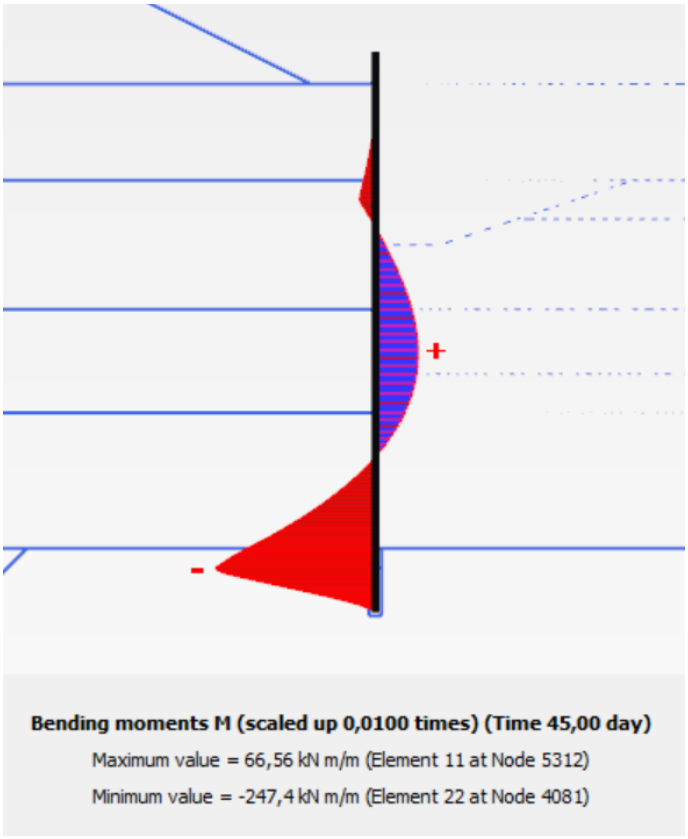


**Figure 5.11:** Bending moment in wall from numerical analysis for section N4.

The moment curves for the other sections are presented in Appendix F together with the shear force for each section. The scaled deformed mesh for section N4 is illustrated in Figure 5.13. As can be seen in the figure the largest deformations occur at the upper part of the retaining wall.

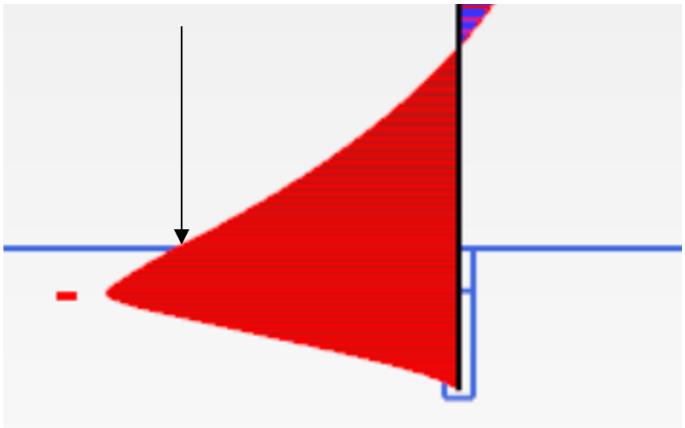


**Figure 5.12:** Illustration of were the assumed maximum moment in the foot.

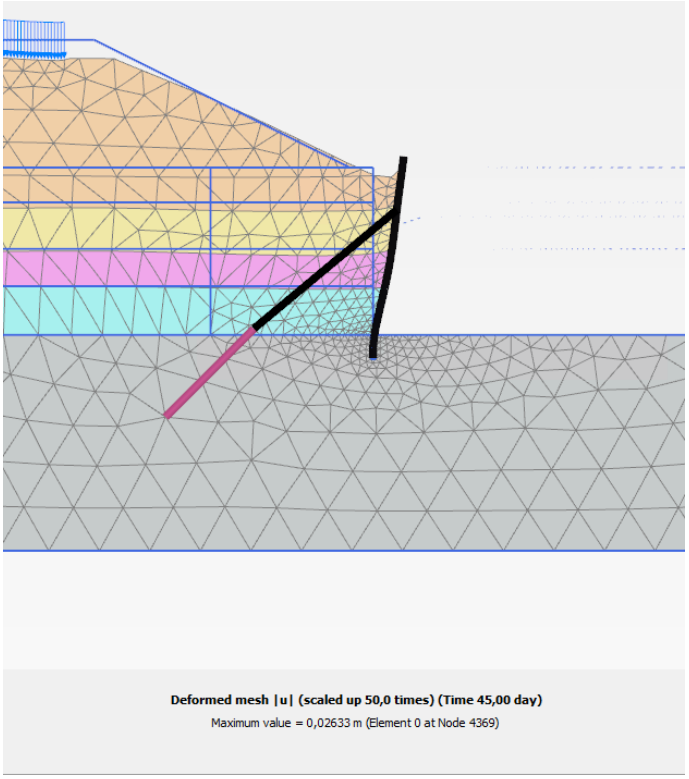


**Figure 5.13:** Deformed mesh for section N4, scaled up 50 times.

### 5.3.2 Sensitivity Analysis on soil parameters

To investigate the degree of influence of various parameters on the outcome of the results, a sensitivity analysis has been performed on the soil layers where each setup gets a final score depending on how sensitive it is to the output results.

The results are presented in Appendix I, and they show that the empirical modulus of elasticity $E_{50}^{ref}$, $E_{oed}^{ref}$, and $E_{ur}^{ref}$ have some effect on the outcome of the results when compared to a safety analysis. The result shows that all scenarios have a safety factor of around 1.7, with $E_{50}^{ref}$ being the most critical parameter with the highest score.

## 5.4 Comparison of Method

The results from the measured values, numerical and analytical calculations are compared in the following chapter. Only the North wall is compared and since there was only load cells installed on four anchors these are the ones compared with numerical and analytical results.

### 5.4.1 Anchor Forces

Anchor forces from analytical calculations, numerical simulations and measured values are compared in Table 5.10 below. As can be seen the fixed end results are approximately 81% of the free end anchor forces. It can be seen that the free end calculations results provides the highest anchor forces, followed by the fixed end calculations. The numerical results are modelled to simulate the measured anchor forces and are thereby similar.

**Table 5.10:** Comparison between anchor forces from analytical and numerical calculations and measured values.

| Anchor | Free end [kN] | "Fixed end" [kN] | Numerical [kN] | Measured [kN] |
|---|---|---|---|---|
| $A1$ | 445.2 | 361.4 | 245.6 | 243.5 |
| $A2$ | 710.0 | 575.4 | 472.4 | 470.2 |
| $A3$ | 735.0 | 594.5 | 469.0 | 477.0 |
| $A4$ | 670.9 | 542.7 | 478.3 | 486.2 |

To relate the analytically and numerically calculated anchor forces with the measured values the ratio is calculated and displayed in Table 5.11. The ratio is determined as the calculated values divided by the measured.

**Table 5.11:** Ratio between calculated and measured values.

| Anchor | Free over measured | Fixed over measured | Numerical over measured |
|---|---|---|---|
| $S_2$ | 1.83 | 1.49 | 0.99 |
| $S_3$ | 1.51 | 1.22 | 0.99 |
| $S_4$ | 1.54 | 1.25 | 1.02 |
| $S_5$ | 1.38 | 1.11 | 1.02 |

The strength capacity against tension for the anchor itself, $F_{t,Rd}$, is presented in Table 3.3 and is 1507 kN. It should be noted that the utilization rate is presented for the SLS case and the utilization rate for ULS and ALS are deemed higher.

**Table 5.12:** Utilization rate of anchors, SLS.

| Anchor | $\eta_{Free}$ | $\eta_{Fixed}$ | $\eta_{Measured}$ |
|---|---|---|---|
| $S_2$ | 30% | 24% | 18% |
| $S_3$ | 47% | 38% | 35% |
| $S_4$ | 49% | 39% | 38% |
| $S_5$ | 45% | 36% | 37% |

### 5.4.2 Moment

The bending moment of the wall is calculated analytically and a numerical analysis is made to simulate the results. The final values for both is displayed in Table 5.13. For both methods the maximal field moment and moment at the foot of the wall are presented. As stated in Section 5.3.1 the numerical moment of the foot is evaluated at the rock level to be similar to the analytical calculations.

**Table 5.13:** Comparison between the maximal field moment and moment at the foot from analytical calculations and numerical simulation. Moment given in kNm/m.

| | **Analytical** | | **PLAXIS** | |
|---|---|---|---|---|
| **Section** | **Field** | **Foot** | **Field** | **Foot** |
| $N1$ | 394.9 | 277.4 | 237.6 | 401.3 |
| $N2$ | 396.4 | 272.8 | 130.4 | 254.2 |
| $N3$ | 328.7 | 217.8 | 137.9 | 371.4 |
| $N4$ | 173.99 | 115.3 | 66.8 | 201.4 |

# 6
# Discussion

The on-site measured anchor forces shows that during excavation and blasting, all anchors have an increased load strain. The north retaining wall's lock-off load was reduced to provide a more significant and detectable difference in load, while the south wall was kept to the design value as reference. All load cells increased in force during excavation, as shown in figure 5.8, where the north load cells (ALC 1-4) increased to a greater extent. It can also be found that the ALC 1-4 shows a larger increase in strain due to blasting inside the shaft compared to the south wall. Despite that the lock-off load of North wall being decreased, the final anchor forces did not reach the initially designed lock-off load which is reasonable thus they are design based on ULS.

Normally the influence off blasting is accounted for in the analytical calculations through the partial coefficient, $\gamma_{ysd,da}$. Though, in the SLS calculation conducted for this thesis the results are aimed to replicate the actual earth pressures and no partial coefficients are used and therefore blasting is not considered. The blasting can influence the anchor force both through the pressure from the blasting itself and through vibrating the sand. It can be discussed how a different surrounding material, e.g. clay, would change these results for sand can be sensitive to vibration. Thus, it can be stated that the blasting inside the excavation influence the anchor forces and should be considered for the ULS/ALS and the design of the anchors.

When pre-stressing the anchor at the desired load effect there is, as mentioned in Section 2.4.3, a loss of load when removing the hydraulic cylinder. This is related to a loss of strain in the anchor, depending on the anchor length, which is accounted for in the normal test-procedure of anchors. For a self-drilled anchor, such as the studied ones, there is an assumed displacement of 3 mm. As can be seen in Section 5.2.1, the loss of load for the measured anchors corresponds to a difference in displacement of approximately 1 mm, which is significantly smaller than the assumed one. Though, it should be noted that 3 mm is assumed based on experience and can be project specific.

As can be seen from the results, that the drilled pile wall can be utilized when designing the anchors in terms of anchor forces. Thereby can the steel amount be reduced. Though, if sheet piles are a possible alternative this still implies less steel material than a drilled pile wall. It can therefore be stated, that when a drilled pile wall is necessary from a production aspect it can be utilized to reduce other dimensions of steel components and thereby the steel amount but if not needed it is not the most steel reducing alternative.

The drilled pile wall for the reference project provides a supported or partially supported foot of the wall. To which extent the wall foot is fixed can be discussed and has to be considered when designing the retaining system. The design engineer had for this studied structure assumed that an added forcing moment at the foot equal to the maximum field moment of the wall could be assumed due to the drilled embedded section for the wall. This assumption is more conservative in comparison to assuming a completely fixed

end. However, it still assumes that the one meter drilled section into rock can be utilized. This is believed to be adequate due to the rock being fractured when drilling and the surrounding cement creating a certain flexibility of the support. When comparing the anchor forces based on analytical results of a partially fixed end against measured values the level of agreement is adequate with a slightly higher result for the analytical result. Compared to the similar studies presented in Section 2.6 it can be seen how the difference between analytical and measured anchor forces are concluded for similar reference projects as well.

If the support would be assumed more rigid the anchor forces would decrease, therefore it can be believed that the assumption of the wall being partially fixed is appropriate to some extent. As can be seen in Section 5.1.4 the bending moment and the moment at the foot of the wall is more sensitive to a reduced strength in the spring stiffness compared to an increase, which gives a more linear development tendency. The tendencies for the waler beam graph follows the same behaviour. The analysis contributes to a prediction of the sensitivity of the rigidity at the foot but assumes that the material parameters remains the same. As stated in the report by Popescu & Ionescu in Section 2.6 the material parameters of the retaining system influence the anchor forces and a change in steel parameters would require a different analysis then the one performed for this thesis.

## 6.1 Model and Method

Modelling the studied excavation in a numerical calculation program, such as PLAXIS 2D, can be a helpful tool. When comparing the results to analytical results the difference between the methods needs to be considered. The analytic calculation is based on Rankine's earth pressure theory while the calculation performed in PLAXIS is based solely on stresses. This implies different soil mechanical behaviours and condition. For an example Rankine's theory assumes the soil to be at failure and requires displacement to develop passive earth pressure while PLAXIS account for displacements and material input parameters. In numerical models the retaining elements are assumed to be locked with no movement. In reality, some movement is inevitable and important for the interplay between the soil and the structure. In PLAXIS, the wall material overlaps the soil which implies that all stress transferring is allocated to the wall and the embedded section into rock. The failure mechanisms are different compared to analytical calculations and measured data. When performing analytical calculations it is assumed that all soil goes to failure at the same time at any point. On the contrary, PLAXIS enables for separate segments of soil to collapse. Furthermore the location of failure can be displayed.

As stated in Section 4.7 the time of each excavation step was inserted in the model but due to that this consolidation was not considered, as the time did not effect the final results. Similarly, no time dependency is accounted for in the analytical calculation, although in "real life" there is a time factor to account for which has influenced the measured anchor forces. Of course, there is several more aspects of the "real case" that is not accounted for in the numerical model such as the excavation bottom and the slope not being totally horizontal. Similarly the excavation steps in PLAXIS attempts to replicate reality but are simplified. Also, no aspects to precipitation and temperature is accounted for in the

numerical and analytical calculations.

When modelling a geotechnical problem in a FEM-program, it is important to choose a soil model that is suitable. An excavation is an un-loading problem and therefore hardening soil deemed a more appropriate model than, for example, Mohr Coulomb. Thus, HS uses stress-strain behaviour combined with a non-linear failure. Further, it uses parameters that consider reloading and swelling of the soil and varies the Young's modulus depending on the stress in the soil. For this thesis, it has been chosen to model the supported section of the retaining wall that is drilled into rock as a zone with two different material properties. By corresponding the numerically calculated anchor forces to the measured ones, the final material properties can be compared to two sections (N2 and N4) with an upper layer consisting of concrete and a lower layer of brittle rock. On the other hand, sections (N1 and N3) have the setup of brittle rock at the top and solid rock at the bottom. It is, and will probably always be, hard to know exactly how each pile is drilled into rock and how much the rock is fractured. Therefore, only assumptions can be made.

The sensitivity analysis of soil layer parameters demonstrates that the model is not particularly sensitive to changes in soil properties. This may be explained by the fact that PLAXIS, in particular, does not put much emphasis on the composition of the surrounding soil, but rather on other aspects that cause the model to fail.

## 6.2 Source of Errors & Recommendations for Further Work

The data collection for the anchor forces was done using load cells read manually by the authors. This required physical access to the load cells and was solved by an self-made optical instrument. The precision of the measurement method is approximated to $\pm$ 3 kN. Furthermore, the measurements was done at chosen times, not done during holidays and not at an exact time interval. The load cells themselves can be sensitive to large differences in temperature, although this is considered to not be the case for these readings. There are load cells on the market that can digitally measure anchor forces, providing a more accurate measurement series and collect a larger amount of data. For future work, using a modern load cells can result in a more precise data collection.

For this study the anchor forces are evaluated based solely on the capacity of the soil and the material of the retaining structure. This can be done as the studied section of project *hamnbanan* has no close buildings or areas sensitive to soil movement. Thus, a similar retaining system can be used in dense areas as well and then the movement of the retaining wall and the displacement of adjacent soil is of greater importance. By increasing the lock-off load, large displacements can be avoided, but to which extend is recommended to be evaluated in further studies.

For further work it is recommended to evaluate the assumption of the rigidity of the support. This can be done by comparing result where the wall is completely fixed or where the surrounding rock is modelled as spring supports. This can provide more a better understanding how the attachment to rock affect the results and how an even more price

result can be calculated for. By installing an inclinometer in or on the retaining wall the movement of the retaining wall can be monitored. This should be installed during the installation of the wall. An inclinometer can provide information about the deflection of the wall which can be used for making the PLAXIS-model more precise with another value to target when modeling the drilled section. Though, the wall is very stiff and has a low utilization rate and therefore deflection is assumed to be quite low.

When testing the anchors and locking them at their lock-off load there is, as mentioned in Section 2.4.3, a small loss in load is to be expected due to movements in the anchor itself. Although when pre-stressing the anchors next to the already locked anchor a certain relaxation can occur in the already stressed anchor and for the soil behind the retaining wall. The numerical calculations are conducted with PLAXIS 2D which thereby is a two dimensional model, that only consider one anchor. As a result, it may be appropriate to model the retaining system in 3D to account for the three-dimensional effects during pre-stressing and then for excavation.

As mentioned before, the accuracy and differences of different material models used in numerical analysis are something to investigate further. This would be specially important if the type of soil differs and consists of e.g. clay, then another material model is most certainly more appropriate. The material input into PLAXIS is based on empirical studies thus, the soil tests where insufficient for the input parameters in the hardening soil model primarily. To provide a more accurate model further testing should be conducted to evaluate soil parameters significant for the studied project. Although, the material parameters for the retaining structures are validated and retrieved from the supplier the material are set to *elastic* in PLAXIS, meaning it will not have a plastic failure in the retaining material. Therefore, failure will only occur in the soil and the wall and anchor will only have deflection.

# 7
# Conclusion

For the measured anchor forces a more significant increase could be seen related to the anchors which had a decreased lock-off load compared to the anchors with a higher one. Measurements from the Anchor Load Cells could establish that the blasting inside the excavation increased the load for all anchors. The anchors with a decreased lock-off load a greater increase from the blasting. The load loss when pre-stressing the anchors is evaluated and deemed lower than expected, although it is claimed that the load loss can influence the lock-load and need to be considered.

To assume an additional forcing moment at the support for a free end calculation is a sufficient method to predict the anchor forces for a drilled pile wall. When analytically calculated results were compared with measured anchor forces at a site in Gothenburg it could be seen that the difference varied between 118 - 56 kN. This implies that the analytical calculations are restrictive if no additional concerns to safety are done. In order to model a drilled pile wall in a numerical analyses the set-up for the embedded support into rock needs to be analysed. Based on the measured anchor forces an analysis of the material strength properties for the embedded section is conducted. It is evaluated that properties simulating brittle rock and concrete are the most correspondent. Thus, the numerical model have a numerous of possible input parameters and aspects to consider.

To summarize, it is possible to take advantage of the drilled pile wall when dimensioning other components of the retaining system, hence the wall is drilled into rock. Thereby, it can be assumed to have a support at the foot which implies that the amount of steel can be reduced. Future research is recommended to include considerations of three dimensional effects and an analysis of other soil materials.

# References


ANP - SYSTEMS GmbH. (2018, 12). *Technical Assessment ANP 76.*

Bentley Systems. (2021). *PLAXIS CONNECT Edition V22.00 Material Models Manual.* Retrieved from https://communities.bentley.com/products/geotech-analysis/w/plaxis-soilvision-wiki/46137/manuals---plaxis

Bergdahl, U., Ottosson, E., & Stigson Malmborg, B. (1993). Plattgrundläggning. In *Plattgrundläggning* (pp. 61–116). AB Svensk Byggtjänst och Statens geotekniska institut.

Brattberg, J. (2011). *DEFORMATIONER KRING SPONT* (Doctoral dissertation, Luleå University of Technology, Luleå). Retrieved from www.ltu.se/shb

Civil Engineering Oraganization. (2016, 8). *Ground Anchor (Earth Anchor) | Types | Anchor Length.* Retrieved from https://engineeringcivil.org/articles/geotechnical-engineering/ground-anchor-earth-anchor-types-anchor-length/

Fredriksson, A., Kullingsjö, A., Ryner, A., & Stille, H. (2018, 2). *Sponthandboken* (Tech. Rep.). Stockholm: Pålkommissionen.

GIKEN LTD. (2022, 2). *Wall and foundation types.*

GLÖTZL. (2019, 3). *GLÖTZL-Anchor Load Cell.* Retrieved from http://www.gloetzl.de/fileadmin/produkte/1%20Messwertaufnehmer/2%20Kraft%20und%20Ankerkraft/Englisch/P_41.00_KN_MF_M_Ankerkraftmessgeber_en.pdf

Hercules Grundläggning. (2022, 2). *Effektiv förankring med stag.* Retrieved from https://hercules.se/grundlaggning/stodkonstruktioner/stag/

Karstunen, M., & Amavasai, A. (2017, 11). *BEST SOIL: Soft soil modelling and parameter determination* (Tech. Rep.). Gothenburg: Chalmers University of Technology.

Keller Group. (2022, 5). *Spont - Stödkonstruktioner.* Retrieved from https://www.kellergrundlaggning.se/expertis/tekniker/spont

Keller Grundläggning. (n.d.). *Stag.* Retrieved from https://www.kellergrundlaggning.se/expertis/tekniker/stag

Knappett, J., & Craig, R. (2012). *Craig's soil mechanics* (8th ed.). New York: Spon Press.

Larsson, R. (1989). *Hållfasthet i friktionsjord* (Tech. Rep.). Linköping: SGI.

Larsson, R. (2008). *Jords egenskaper* (Tech. Rep.). SGI.

Naturvårdsverket. (2022, 2). *Territoriella utsläpp och upptag av växthusgaser.* Retrieved from naturvardsverket.se/data-och-statistik/klimat/

vaxthusgaser-territoriella-utslapp-och-upptag/

Popa, H., & Batali, L. (2010, 3). Using Finite Element Method in geotechnical design. Soil constitutive laws and calibration of the parameters. Retaining wall case study. *WSEAS Transactions on Applied and Theoretical Mechanics Journal*, *Volume 5*, 177–186.

SGI. (2022, 3). *Jords hållfasthet.* Retrieved from https://www.sgi.se/sv/kunskapscentrum/om-geoteknik-och-miljogeoteknik/geoteknik-och-markmiljo/jordmateriallara/skjuvhallfasthet/

Skanska. (2020, 1). *Redogörelse Hamnbanan etapp Eriksberg-Pölsebo Göteborg, Västra Götalands län Trafikverket* (Tech. Rep.). Göteborg: Trafikverket.

Skanska AB. (n.d.). Konstruktionsdelar.

Skanska Sverige AB. (2021). *ZON 2B Temporär stödkonstruktion för tunnel Beräkningar tillfällig spont Godkänd bygghandling* (Tech. Rep.). Göteborg.

SSAB AB. (2022, 2). *RD® pile retaining walls.* Retrieved from https://www.ssab.com/products/steel-categories/infrastructure/products/retaining-walls-rd-pile-wall?dcFilter=&dcSearch=

StruSoft. (2022, 6). *Frame Analysis.* Retrieved from https://strusoft.com/software/structural-engineering-software-win-statik/frame-analysis/

Surarak, C., Likitlersuang, S., Wanatowski, D., Balasubramaniam, A., Oh, E., & Guan, H. (2012, 8). Stiffness and strength parameters for hardening soil model of soft and stiff Bangkok clays. *Soils and Foundations*, *52*(4), 682–697. doi: 10.1016/j.sandf.2012.07.009

Swedish Standard Institute. (2022). *Eurocode 7: Geotechnical design-Part 1: General rules.* Retrieved from www.sis.se

Swedish Standards Institute. (2016). *Testing of geotechnical structures - Anchorage SS 27104:2016.* Retrieved from https://www.sis.se/std-8018623

Trafikverket. (2015, 5). *Planbeskrivning. Hamnbanan Göteborg, dubbelspår Eriksberg-Pölsebo.*

Trafikverket. (2016, 2). *Trafikverkets tekniska råd för geokonstruktioner - TR Geo 13.* Trafikverket.

# A

# Appendix: Earth pressures

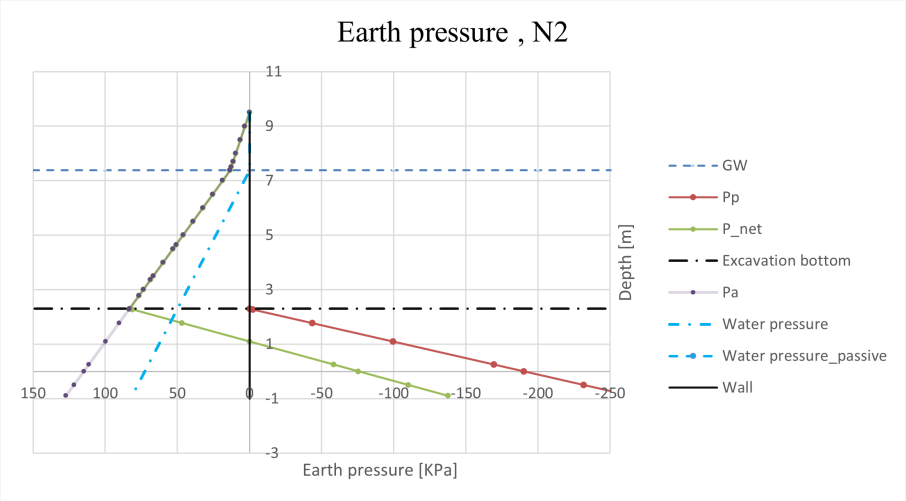


**Figure A.1:** Earth pressures acting on the wall, section N2.

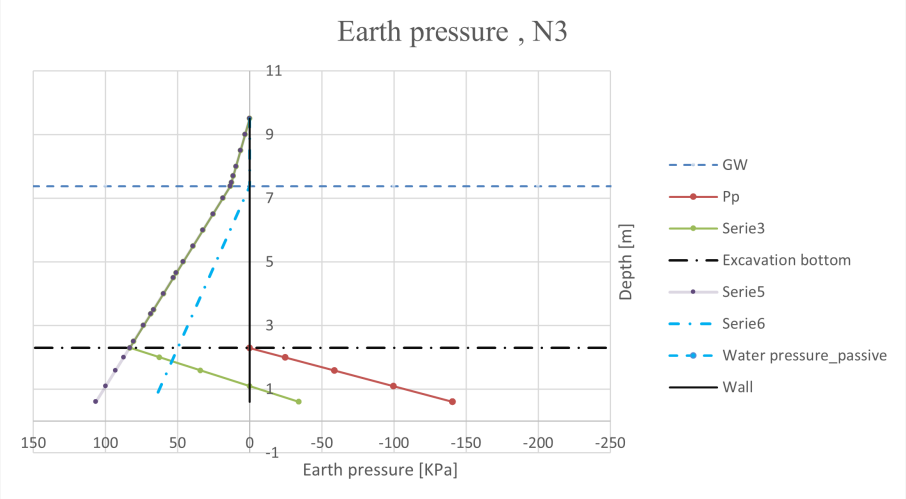


**Figure A.2:** Earth pressures acting on the wall, section N3.

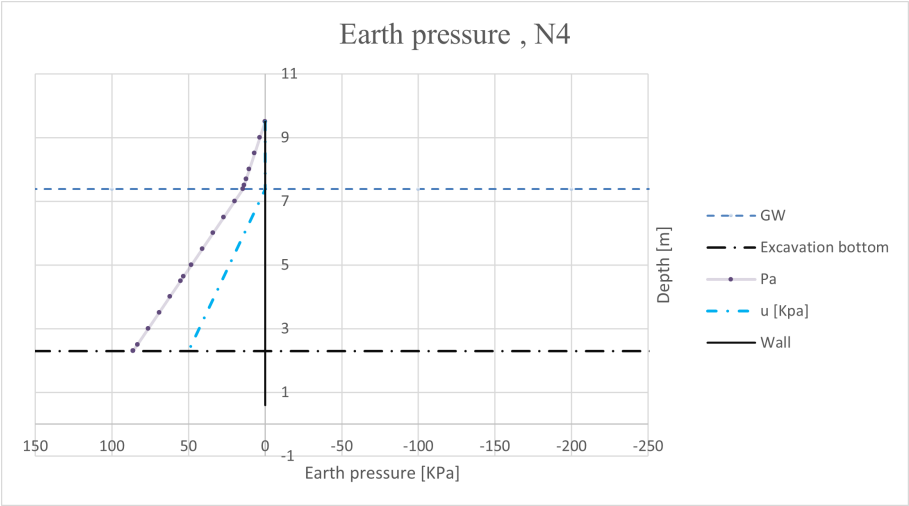


**Figure A.3:** Earth pressures acting on the wall, section N4.

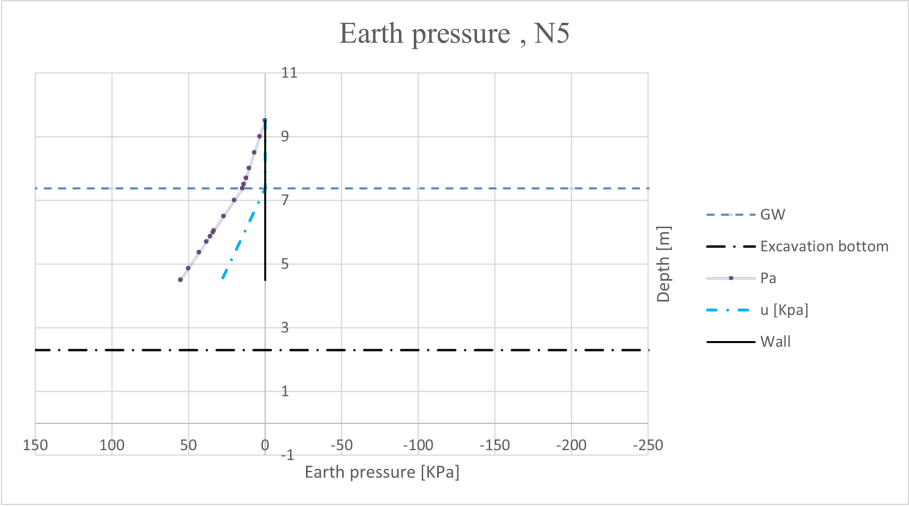


**Figure A.4:** Earth pressures acting on the wall, section N5.

# B

# Appendix: Rock surface based on drilled pile wall.

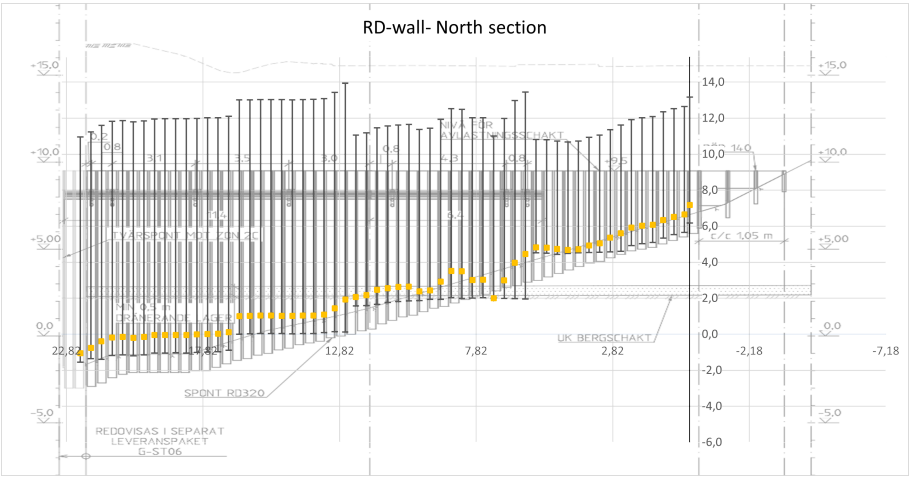


**Figure B.1:** Rock surface model with pile wall level based on drill-protocols, North wall

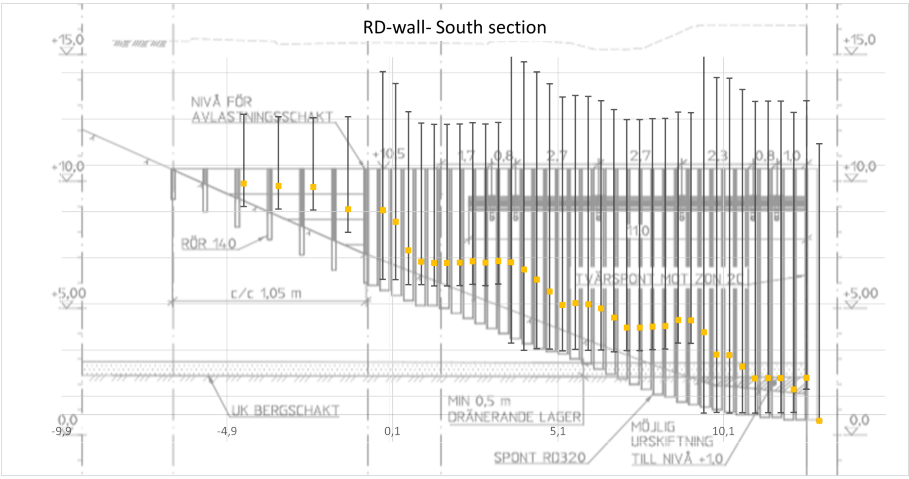


**Figure B.2:** Rock surface model with pile wall level based on drill-protocols, south wall

# C

# Appendix: Read values for the earth pressure coefficients.

The $K_A$ and $K_P$ are evaluated and read as shown in the figure below. $\beta$ are the inclination of the adjacent slope and are set to ca 27 degrees. For the ULS and ALS calculations done by the designing engineer the $K_p$ are set to a maximum of 5 to not over estimate the passive pressure contribution. Although, for the SLS calculation of this report 6.52 are used according to the graph. For $K_P$ the graph for a horizontal surface are used since bottom of excavation are assumed to be horizontal.

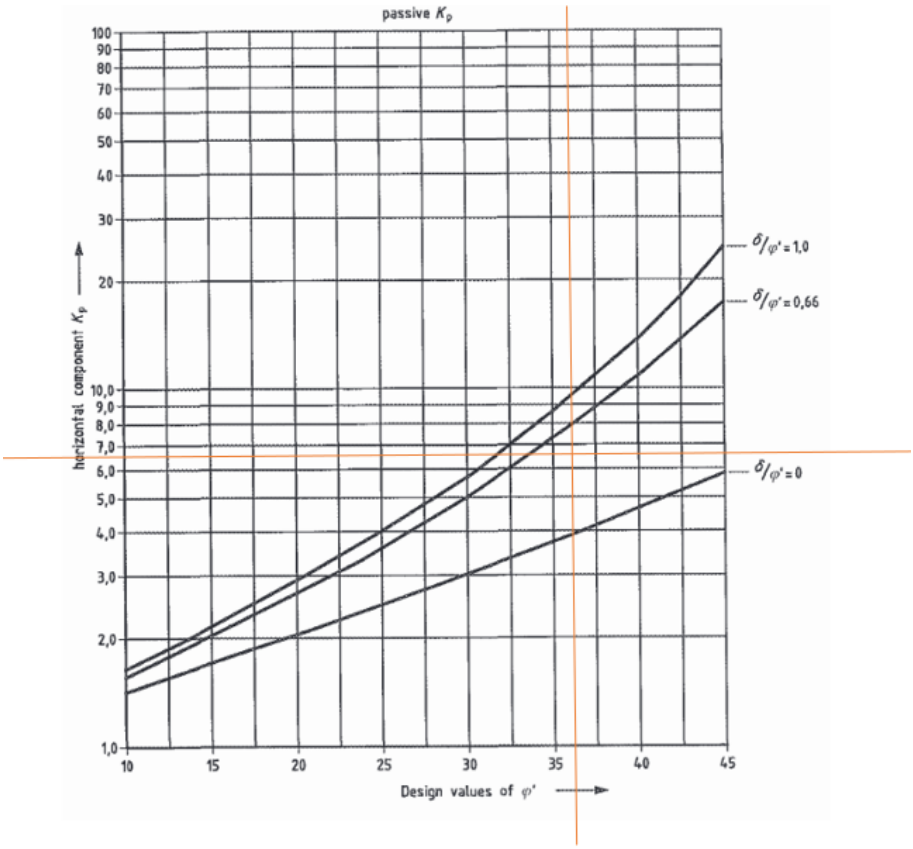


Figure C.2.1 — Coefficients $K_p$ of passive earth pressure: with horizontal retained surface ($\beta = 0$)

**Figure C.1:** Example of read values for earth pressure coefficient

**Table C.1:** Read Ka & Kp values

| | K_A | K_P |
|---|---|---|
| N1 | 0.35 | 6.52 |
| N2 | 0.38 | 6.52 |
| N3 | 0.38 | 6.52 |
| N4 | 0.38 | 6.52 |
| N5 | 0.38 | 6.52 |

# D

# Locations of ACL of south wall

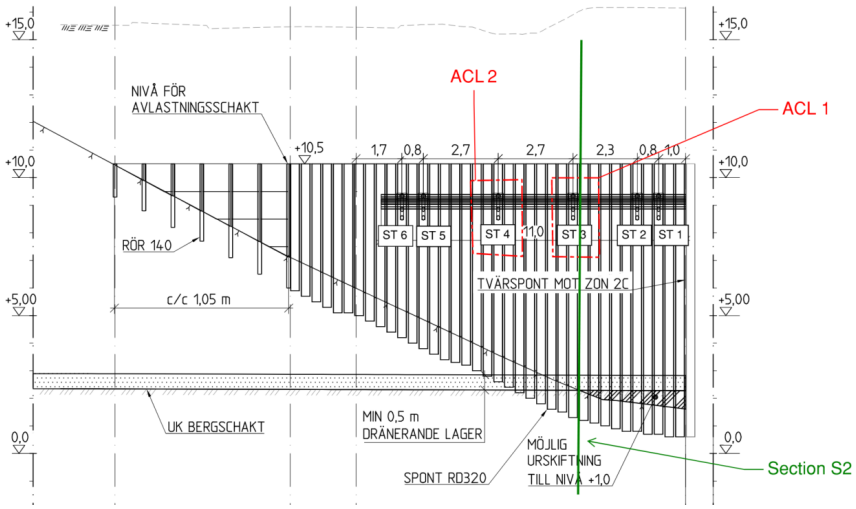


**Figure D.1:** The location of the anchor loads cell´s on the south side, also the calculated sections location.

# E

# Moment and Shear force of analytical calculations for section N2-N5

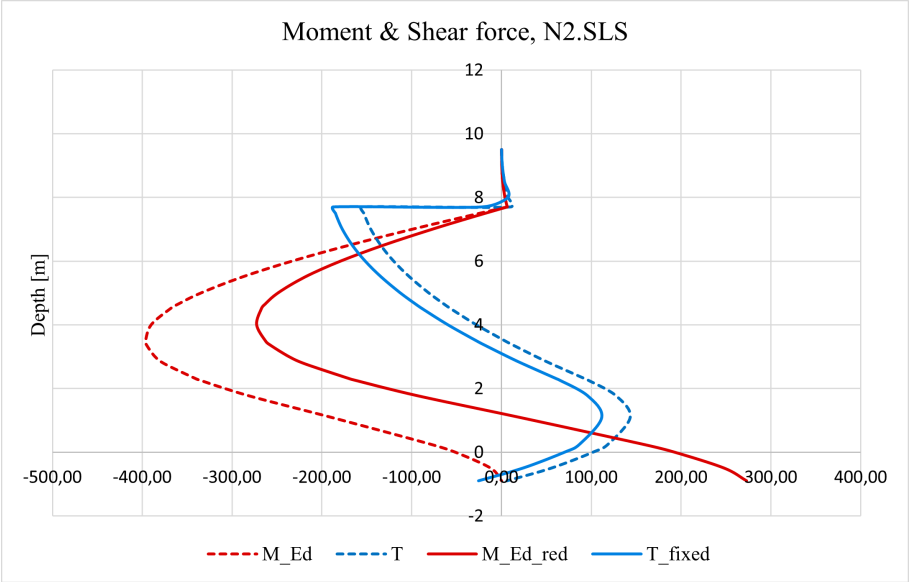


**Figure E.1:** Moment and shear force for section N2

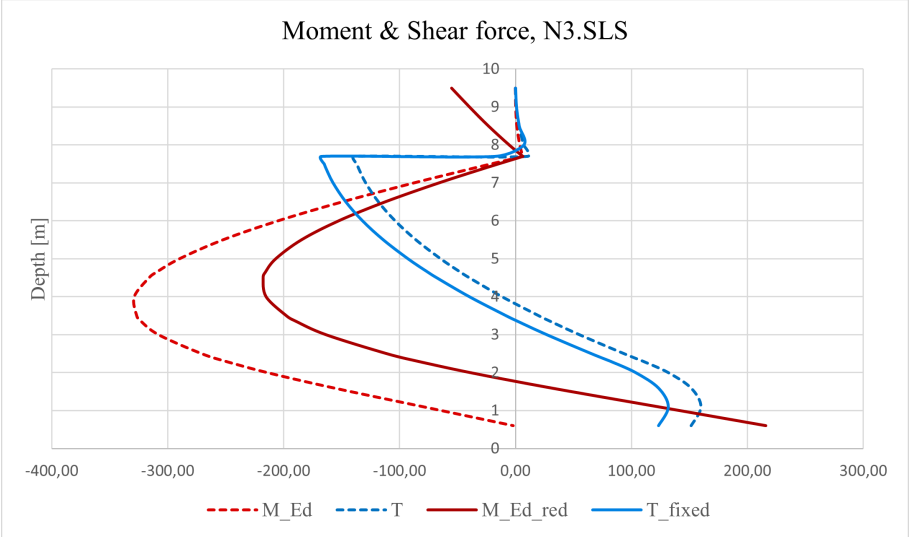


**Figure E.2:** Moment and shear force for section N3

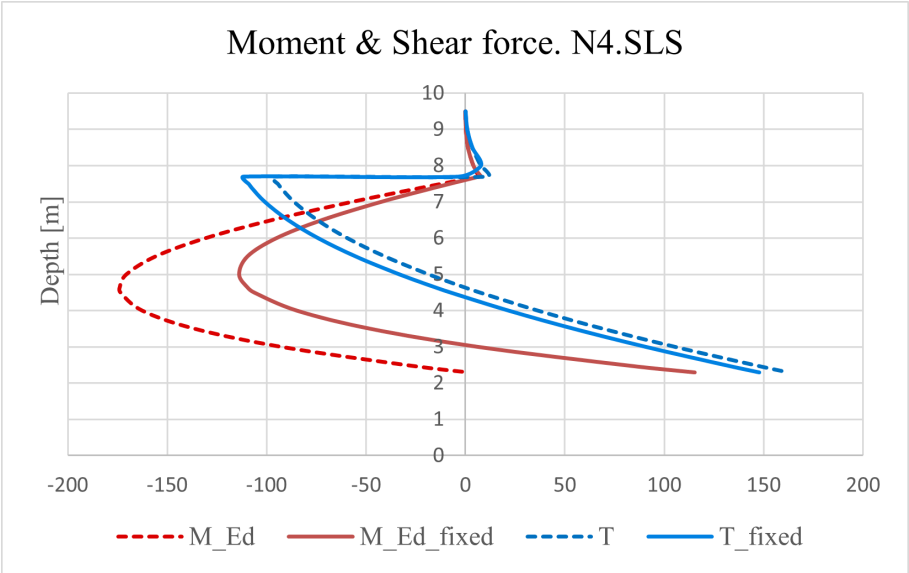


**Figure E.3:** Moment and shear force for section N4

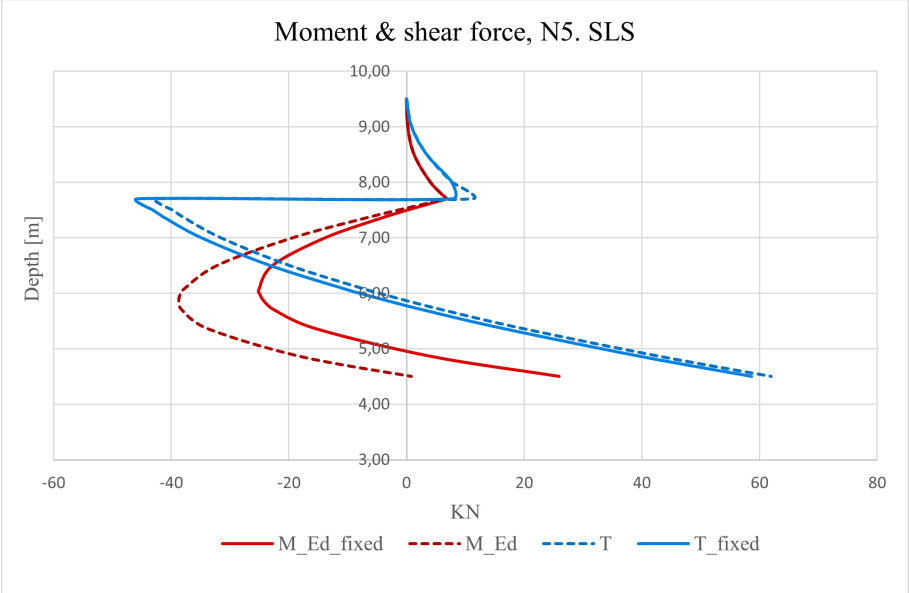


**Figure E.4:** Moment and shear force for section N5

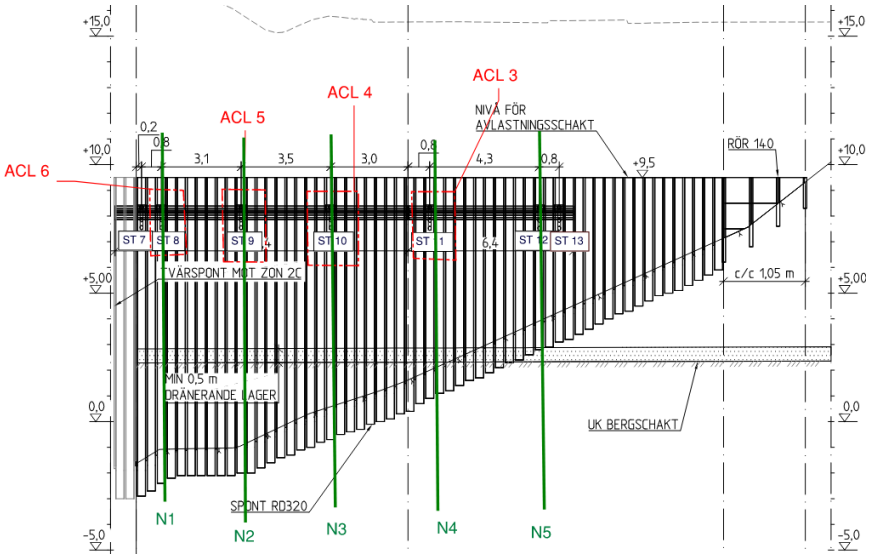


**Figure E.5:** The location of the anchor loads cell´s on the north side, also the calculated sections location.

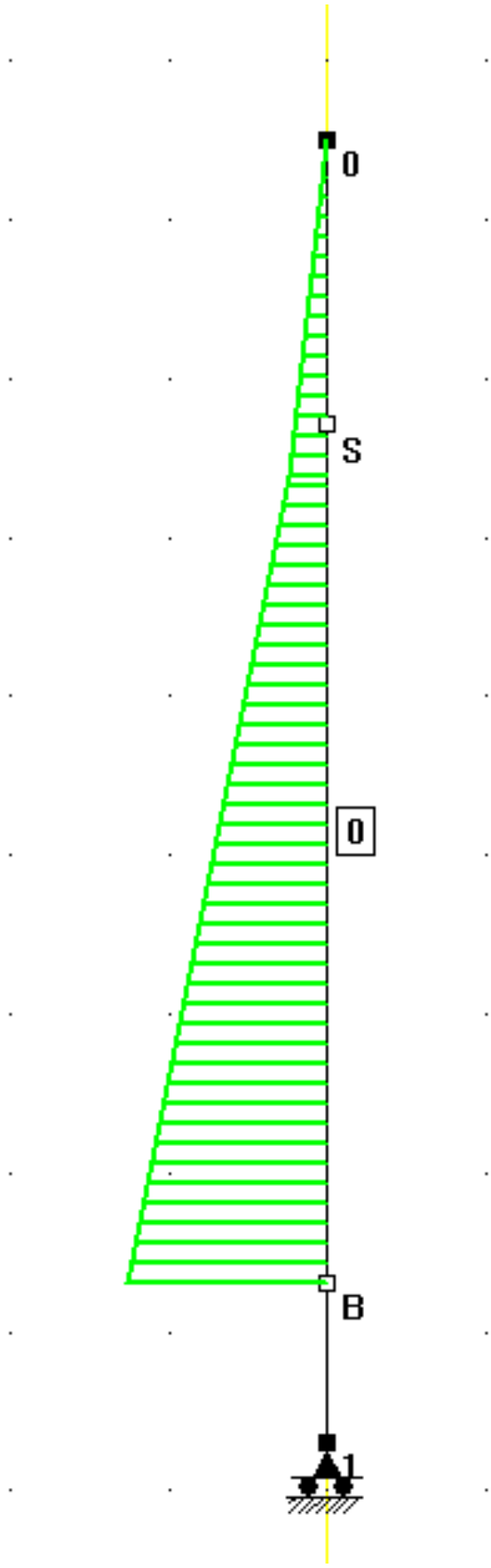


**Figure E.6:** The set-up in beam program with load

# F

# Bending momenet & Shear forces

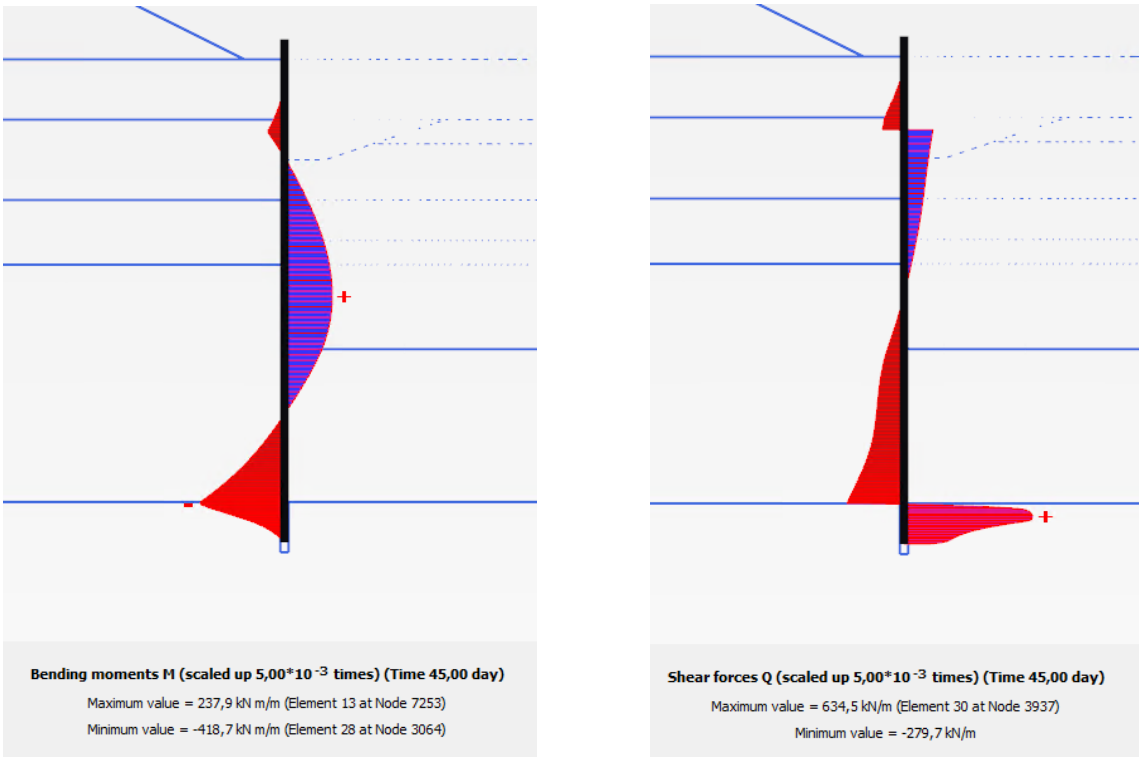


**Figure F.1:** Bending moment (left) and shear forces (right) when full excavation is performed in PLAXIS regarding section N1

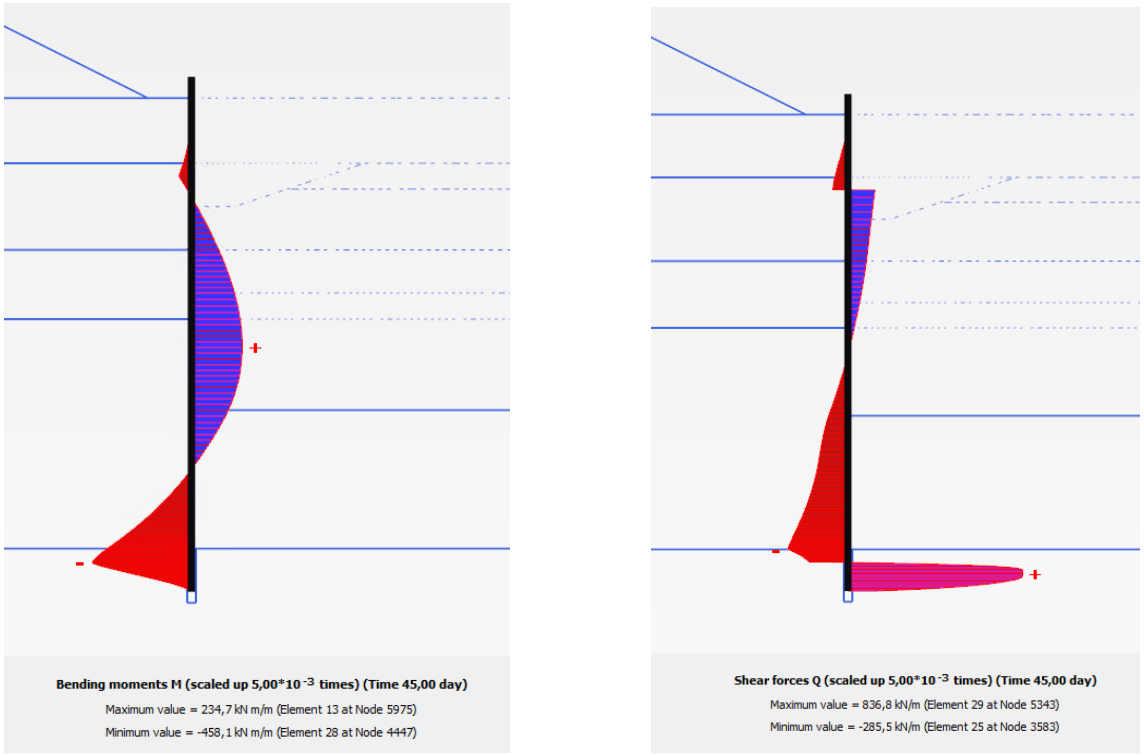


**Figure F.2:** Bending moment (left) and shear forces (right) when full excavation is performed in PLAXIS regarding section N2

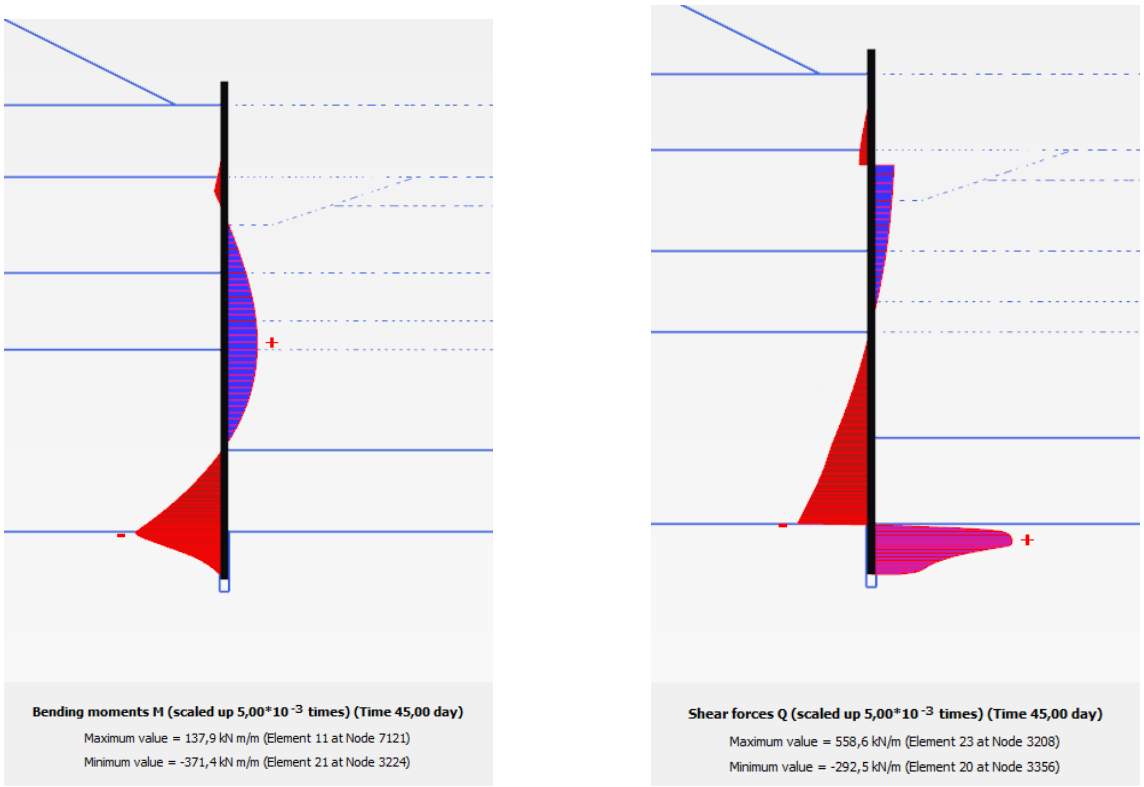


**Figure F.3:** Bending moment (left) and shear forces (right) when full excavation is performed in PLAXIS regarding section N3

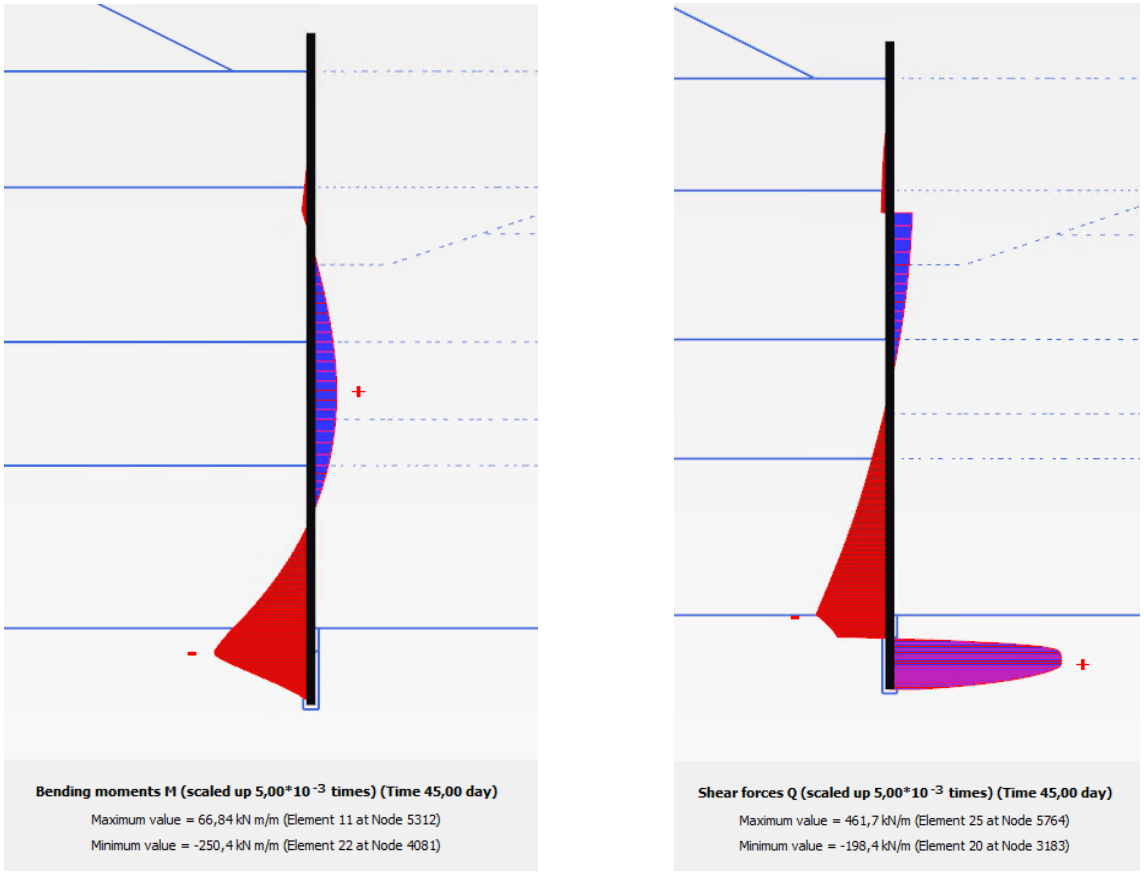


**Figure F.4:** Bending moment (left) and shear forces (right) when full excavation is performed in PLAXIS regarding section N4

# G
# Compared Anchor forces

Following is the compared anchor forces of the analytical calculations and the numerically simulated values.

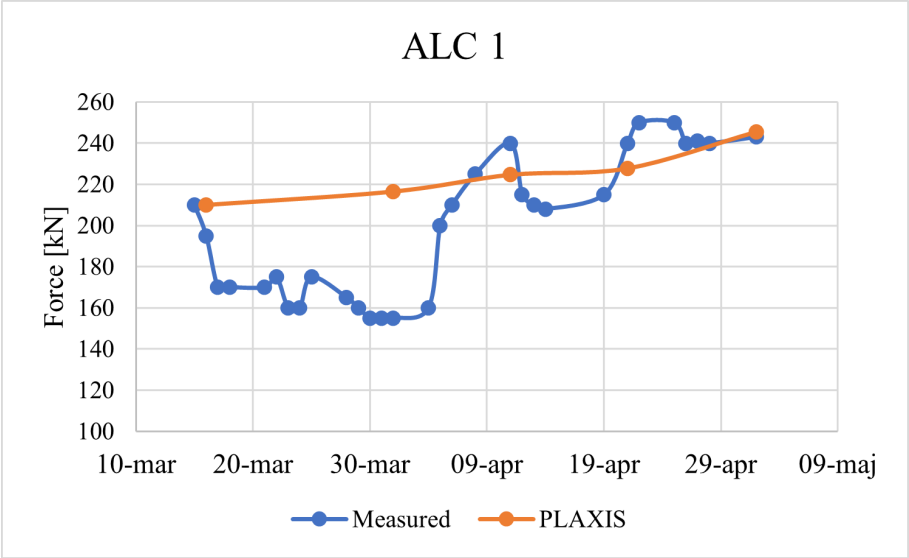


**Figure G.1:** Comparison between measured forces and simulated from PLAXIS for ALC 1.

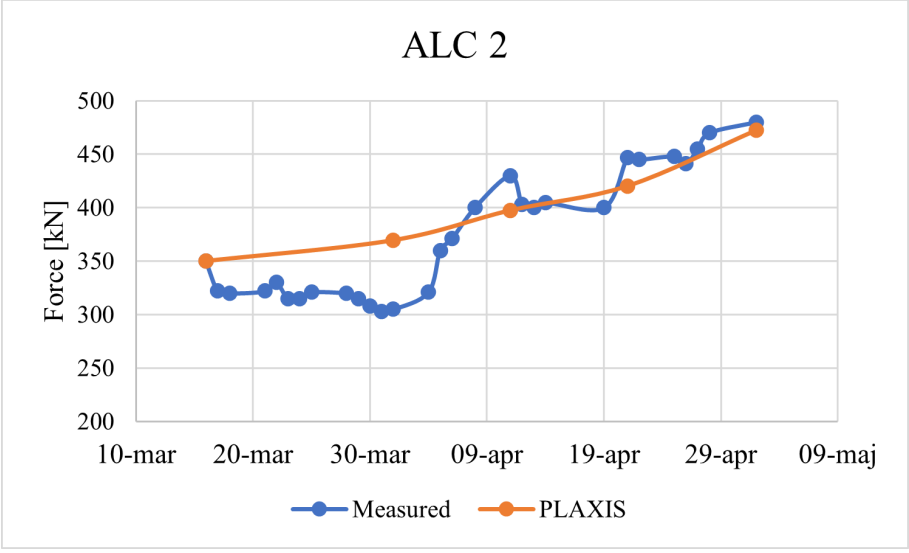


**Figure G.2:** Comparison between measured forces and simulated from PLAXIS for ALC 2.

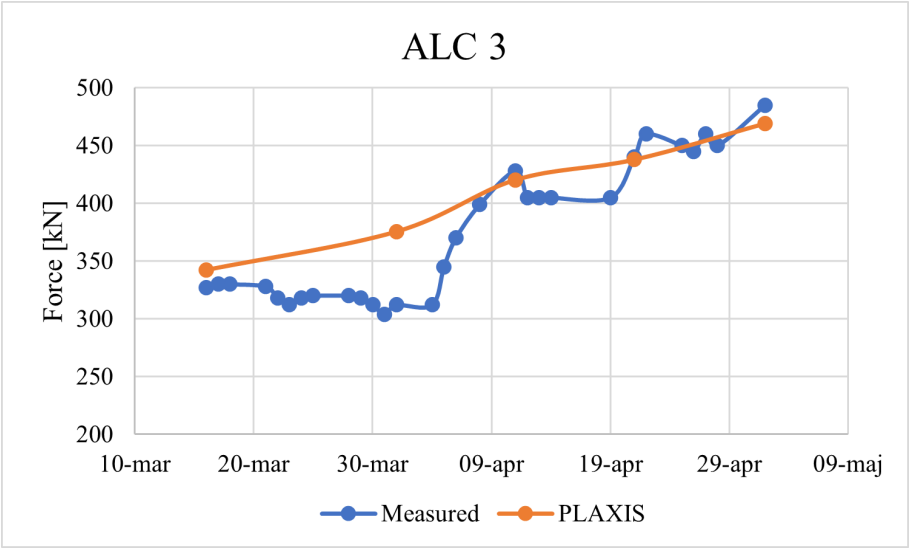


**Figure G.3:** Comparison between measured forces and simulated from PLAXIS for ALC 3.

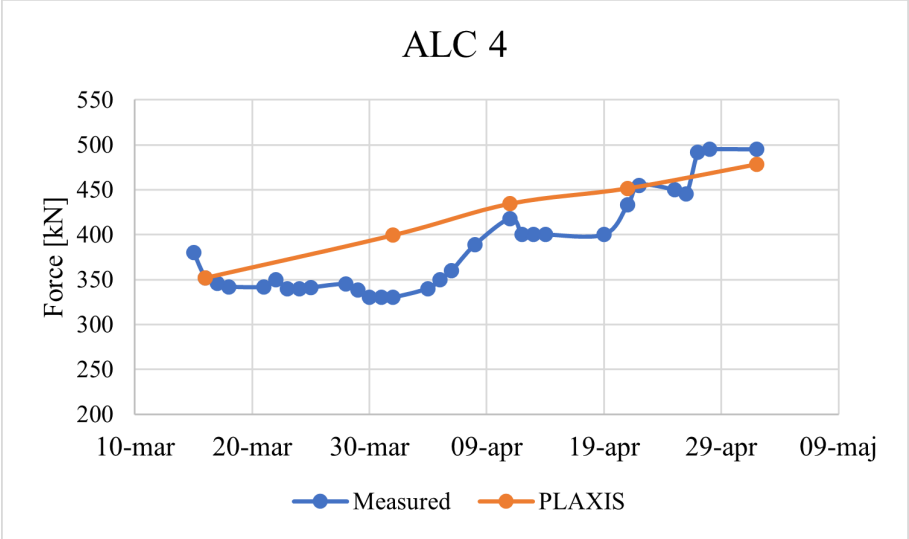


**Figure G.4:** Comparison between measured forces and simulated from PLAXIS for ALC 4.

# H
# Conversion factor

The conversation factor is evaluated as:

$$\eta = \eta_1 \cdot \eta_2 \cdot \eta_3 \cdot \eta_4 \cdot \eta_5 \cdot \eta_5 \cdot \eta_6 \cdot \eta_7 \cdot \eta_8 \tag{H.1}$$

**Table H.1:** The determined conversion factor according to Eurocode (Swedish Standard Institute, 2022).

| $\eta$ | value |
|---|---|
| $\eta_{1,2,3,4}$ | 0.96 |
| $\eta_{5,6}$ | 1.15 |
| $\eta_7$ | 1 |
| $\eta_8$ | 1 |
| $\eta_{mean}$ | 1.017 |

The conversion factor is evaluated and decided to be 1.1.

# I

# Sensitivity Analysis




**Figure I.1:** Sensitivity analysis with respect to elastic modulus for each soil layer.

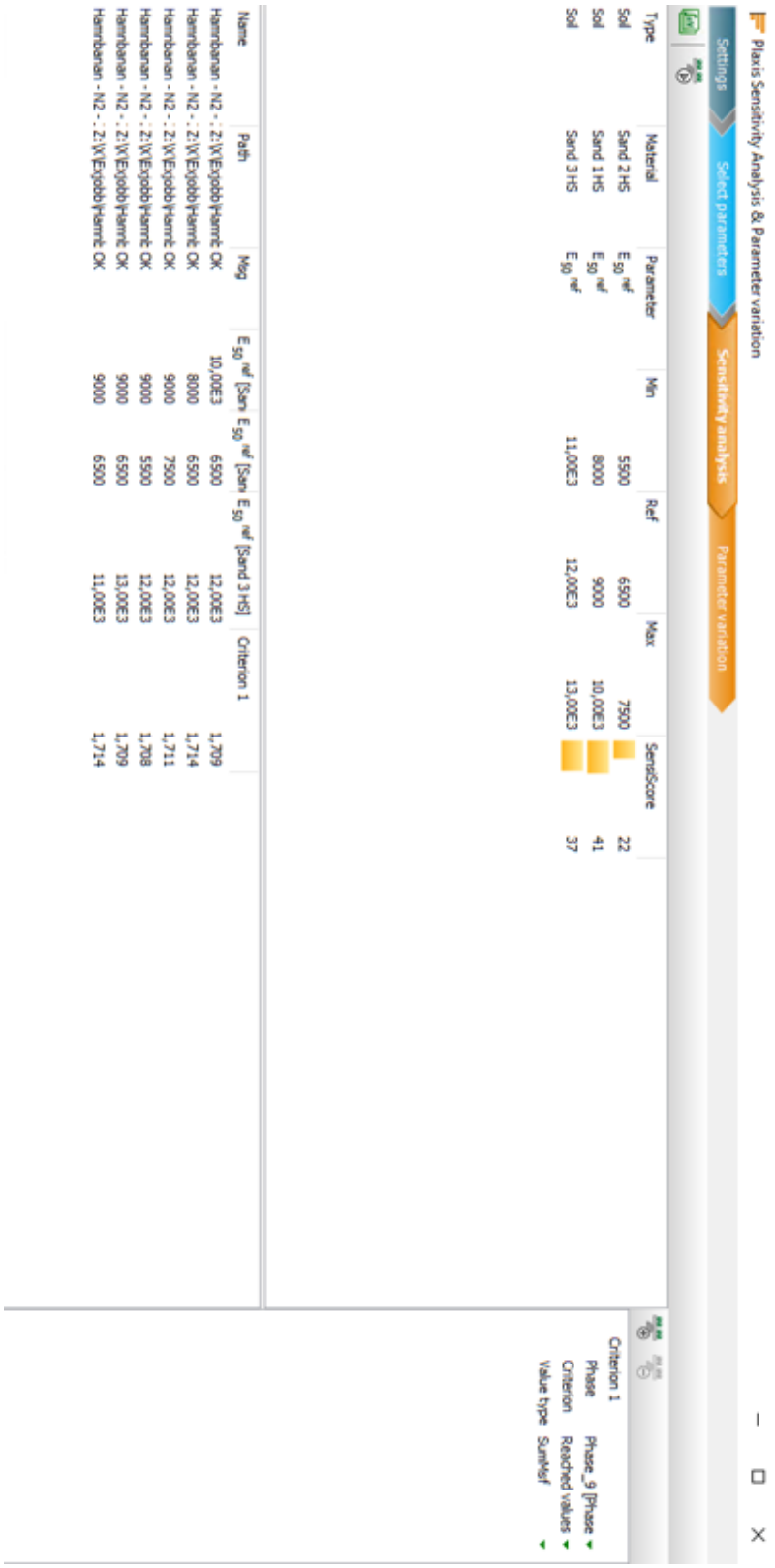


**Figure I.2:** Sensitivity analysis with respect to $E_{50}^{ref}$ for soil layer 1-3.

**DEPARTMENT OF SOME SUBJECT OR TECHNOLOGY**
**CHALMERS UNIVERSITY OF TECHNOLOGY**
Gothenburg, Sweden
www.chalmers.se


CHALMERS
UNIVERSITY OF TECHNOLOGY